

# Association Euratom - Risø National Laboratory annual progress report for 1997

**Lynov, Jens-Peter; Singh, Bachu Narain**

*Publication date:*
1998

*Document Version*
Publisher's PDF, also known as Version of record

Risø-R-1070(EN)

# Association Euratom - Risø National Laboratory Annual Progress Report 1997

**Edited by J. P. Lynov and B. N. Singh**

**Abstract** The programme of the Research Unit of the Fusion Association Euratom - Risø National Laboratory covers work in fusion plasma physics and in fusion technology. The fusion plasma physics group has activities within development of laser diagnostics for fusion plasmas and studies of nonlinear dynamical processes related to electrostatic turbulence and turbulent transport in magnetised plasmas. The activities in technology cover investigations of radiation damage of fusion reactor materials. These activities contribute to the Next Step, the Long-term and the Underlying Fusion Technology programme. The technology activities also include contibutions to macrotasks carried out under the programme for Socio-Economic Research on Fusion (SERF). A summary is presented of the results obtained in the Research Unit during 1997.

ISBN 87-550-2438-6
ISBN 87-550-2439-4 (Internet)
ISSN 0106-2840
ISSN 1396-3449

# Contents

# 1. Preface

The activities in the Research Unit cover two main areas:

**Fusion Plasma Physics** which includes:

- *Laser plasma diagnostics.* Development of laser diagnostics for spatially localised turbulence measurements. In collaboration with IPP Garching successful measurements have been performed on the W7-AS stellarator with a new collective scattering diagnostic.
- *Nonlinear dynamics of fusion plasmas*. For the interpretation of the results from the laser diagnostic, extensive computer simulations are carried out of the plasma density fluctuations under various types of electrostatic turbulence. These simulations are also used for studies of coherent structures and their influence on turbulent transport.

**Fusion Technology** which includes:

- Experimental and theoretical investigations of the effects of irradiation on the microstructural evolution and on the physical and mechanical properties of metals and alloys relevant to the Next Step, the Long Term and Underlying Fusion Technology Programme.
- Contributions to macro-tasks carried out under the programme of Socio-Economic Research on Fusion (SERF).

# 2. Fusion Plasma Physics

## 2.1 Introduction

The activities in this area have been carried out under the Plasma Physics and Fluid Dynamics Programme in the Optics and Fluid Dynamics Department. The main objective of the research is to contribute to the understanding of turbulent transport in fusion plasmas. In the work towards this objective, the programme interacts with other activities in the department in the fields of optics and fluid dynamics to the mutual scientific benefit of the projects involved.

The main results obtained during 1997 can be summarised as follows: In collaboration with the Max-Planck-Institute for Plasma Physics in Garching, Germany, the first successful measurements with Risø's laser diagnostic on the Wendelstein 7-AS stellarator of two-point correlations in plasma turbulence have been carried out. These experimental investigations were supported by a number of theoretical and numerical studies. Theoretical studies have been carried out on the spectral analysis of plasma turbulence time series, and fully three-dimensional numerical simulations of various types of plasma turbulence have been conducted. New results have also been obtained on particle diffusion in electrostatic turbulence and on the theoretical description of inward transport via the concept of 'Turbulent Equipartition'.

A brief description is included of two external projects, which are derived from the main scientific programme. These projects are: 1) Pellet injectors and 2) Industrial spin-off of laser anemometers for wind turbines.

# 2.2 Laser Plasma Diagnostics

### 2.2.1 Collective scattering turbulence measurements at the W7-AS stellarator

*W. Svendsen, M. Saffman, B. Sass, J. Thorsen*

Work continued on collective scattering turbulence measurements on the W7-AS stellarator experiment at the Institute for Plasma Physics in Garching. The instrument, which is based on a two-point correlation measurement technique[1], has been designed to give enhanced spatial resolution of large scale turbulence. Relatively small scale turbulence is measured at two points in the plasma. When looking at small scales the spatial extent of the measurement volume can be reduced, which improves the spatial resolution. The two points are separated by a distance corresponding to the large scale turbulence that is important for transport in the plasma. Measuring the cross-correlation of the signals from the two measurement points allows the group velocity at large scales to be inferred. The limitation to the spatial resolution that can be achieved depends on the presence of measurable fluctuations in the plasma at small scales.

During 1997 measurements were performed at wavenumbers lying in the range of roughly 10 to 150 $cm^{-1}$. A typical example of the temporal variation of the measured turbulence intensity is shown in Figure 1.

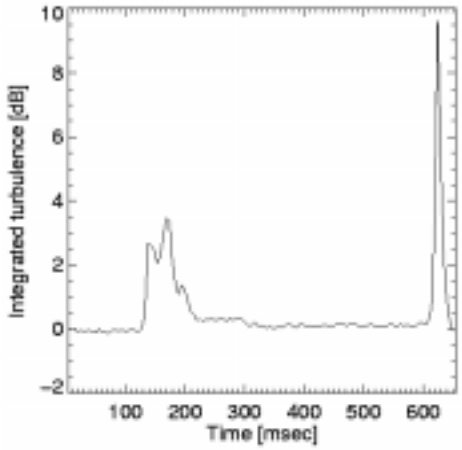


Figure 1. Time resolved turbulence spectra showing high turbulence intensity at the beginning and end of the discharge. Data are from shot 41908, and were obtained at 22 $cm^{-1}$.

It is seen that there are strong bursts of turbulence at the onset and cessation of the discharge, as well as a considerably lower turbulence level from 200-300 msec. The strong turbulence levels at the ends of the discharge window were observable at large wavenumbers up to about 150 $cm^{-1}$. On the other hand the lower turbulence levels occurring under stationary, or quasi stationary, plasma conditions generally required measurements at smaller wavenumbers, of not more than 20 - 40 $cm^{-1}$ in order to obtain good signal to noise ratios.

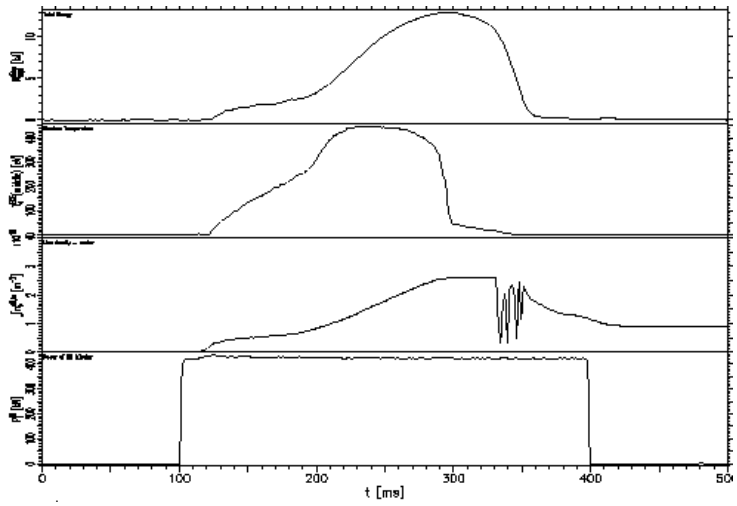


Figure 2**.** W7-AS plasma discharge number 40774 of 29 September 1997. From top to bottom: diamagnetic energy [kJ], electron temperature [eV], line integrated electron density [$10^{-19}$ $M^{-2}$], and neutral beam injection power [kW].

Results obtained when measuring turbulent fluctuations centered at $\kappa$ = 36 $cm^{-1}$ are shown in the following figures. At these wavenumbers the spatial extent of the measurement region corresponded to a long pencil with diameter of 4 mm, and characteristic length of order one meter. Some parameters of a plasma discharge with neutral beam injection at W7-AS are shown in Figure 2.

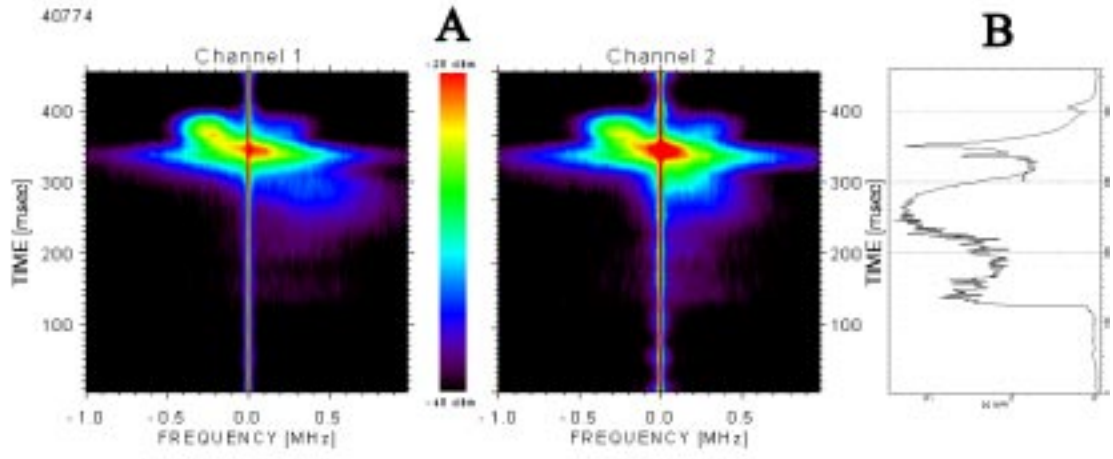


Figure 3. (A) Measured power spectrum vs. time and (B) H-alpha signal.

The discharge lasts about 400 msec, with the highest temperatures and densities obtained in the latter part of the discharge. Measurement results from the discharge are shown in Figure 3. The measuring points were placed in the upper half of the plasma, and were separated in the poloidal direction by 13.8 mm. At each measuring location, fluctuations centred at $\kappa$ = 36 $cm^{-1}$ and with a spread in $\kappa$ of about 10 $cm^{-1}$ were detected. The beams were oriented to measure fluctuations travelling in the poloidal direction. Figure 3A illustrates the temporal development of the measured power spectrum in the two channels. A strong signal is obtained at the end of the discharge. The strong central peak in the power spectrum is due to a small parasitic leakage between the local oscillator

and primary beams. Figure 3B shows the H-alpha diagnostic signal which is an indicator for the particle and energy flow out of the plasma. The sharp peak in the H-alpha signal indicating a burst of energy out of the plasma occurs at the time where the collective scattering turbulence signal is largest.

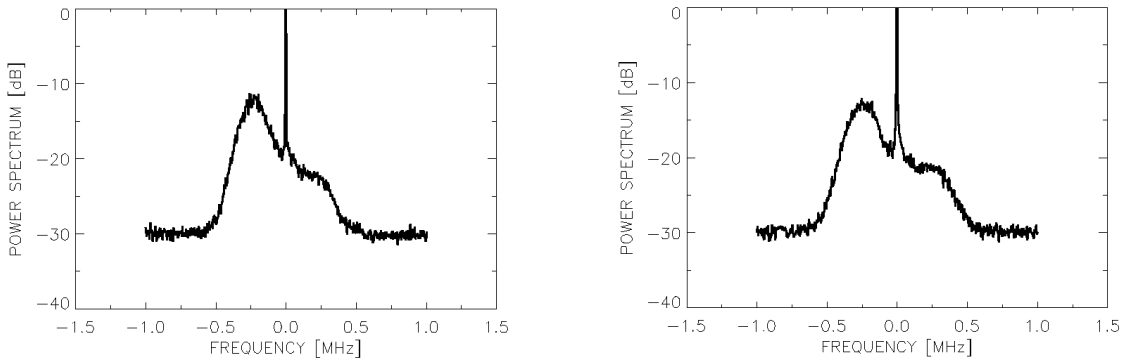


Figure 4. Power spectrum measured at t=370 msec.

The power spectrum has a maximum at about -250 kHz as seen in Figure 4. This corresponds to a poloidal phase velocity of about 450 M/sec, in the electronic diamagnetic drift direction.

The power spectra are asymmetric, with the largest part of the turbulence intensity corresponding to propagation in the electron diamagnetic drift direction. It can also be seen in Figure 3 that the direction of propagation of the major part of the turbulence changes during the plasma discharge.

It is interesting to note that the observation of asymmetric turbulence spectra is evidence for a degree of spatial localisation less than the size of the plasma. If this were not the case, we would expect equal contributions from above and below the plasma centre line, and hence symmetric spectra. Partial localisation is obtained despite the fact that the characteristic length of the measurement volume defined by the optical set-up is of the size of the plasma. Correlation analysis of this, as well as other data, in order to extract the effective group velocity of the fluctuations is currently in progress.

1. L. Lading, M. Saffman, S.G. Hanson, and R.V. Edwards, *J. Atmos. and Terr. Phys*. **58**, 1013 (1996).

### 2.2.2 Theoretical analysis of two-point collective scattering correlation functions using a drift wave model

*N. Heinemeier and M. Saffman*

The principle behind two-point collective scattering as a turbulence diagnostic has previously[1] been described in detail. The basic idea is that small-scale fluctuations are measured at two adjacent points in the plasma. A localised fluctuation at the first point will give a certain detector signal, and as the fluctuation propagates to the second measurement point, the same signal is recorded by the second detector. Since the distance is known, the time delay between identical signals can

be used to estimate the group velocity. The comparison of signals is done by time-crosscorrelation. In principle, the crosscorrelation function will have a sharp peak at the time-of-flight, but the function is distorted by the effects of fluctuation decay and instrumental uncertainty in the measurement wavenumber. Hence, it is preferable to have an expected correlation function that can be fitted to the measured function, allowing the extraction of the group velocity. Such a function has previously[1] been calculated for measurements with collective scattering in a normal fluid.

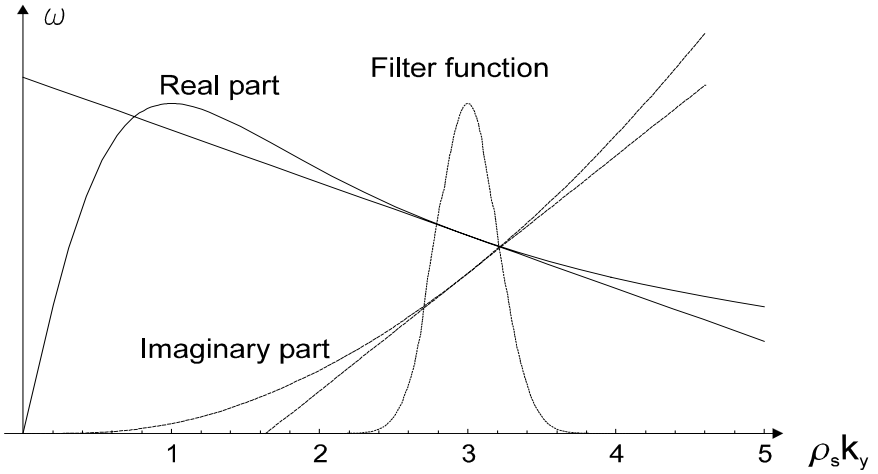


Figure 5. The real and (negative) imaginary part of the dispersion relation for drift waves. The so-called filter function is determined by the experimental setup. It determines which wavenumbers contribute to the signal, and is shown here for a typical setup of the collective scattering diagnostic at W7-AS. Also shown are the linear approximations to the real and imaginary parts of the dispersion relation. The approximation is seen to be good for the wavenumbers allowed by the filter function.

We have calculated the expected crosscorrelation function for fluctuations in a plasma, using a drift wave model. The crosscorrelation can be written[2,3] as an integral of the space-time fluctuation power spectrum times a filter function that describes the extent of the wavenumber spectrum that is measured. The time evolution of the power spectrum can be described using the appropriate dispersion relation. From the linearized Hasegawa-Wakatani equations, it is possible to obtain such a relation for drift waves[4]. In our analysis, we have assumed infinite plasma conductivity, which corresponds to neglecting the growth towards instability. Instead, we have concentrated on the damping due to ion viscosity. The starting point is thus a dispersive and dissipative relation between frequency and wave number. To obtain an analytic expression for the crosscorrelation function, we linearize the real and imaginary parts of the dispersion relation around the measurement wavenumber. If the filter function is not too broad, this can be done with only a small error.

The resulting crosscorrelation is basically a Gaussian function with a peak at the time-of-flight and a width proportional to the beam diameter. This is multiplied by an exponential decay term, resulting in a displacement of the peak towards shorter times. The different decay times of fluctuations at different wavenumbers alters the shape of the

function even further. Due to the long extension of the measurement volume signals may arise from waves propagating in both the electron and ion diamagnetic drift directions, resulting in peaks at both positive and negative time displacements.

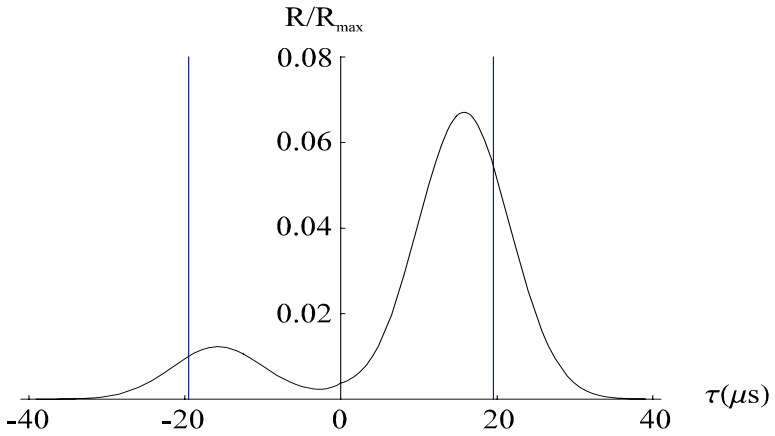


Figure 6. The expected crosscorrelation function, normalised by the maximum crosscorrelation for the case of no decay. The function is shown for realistic plasma and beam parameters, except the decay constant, which has been exaggerated to exhibit the effect of fluctuation decay on the crosscorrelation more clearly. The vertical lines mark the time-of-flight of the fluctuations, and the crosscorrelation is seen to peak at shorter absolute times. The function is shown for weight factors 0.7 and 0.3 of fluctuations propagating in the positive and negative measurement directions, respectively.

1. Association Euratom - Risø National Laboratory Annual Progress Report 1995.
2. L. Lading, R. V. Edwards and M. Saffman, *Opt. Lasers in Eng*. **27**, 531 (1997).
3. L. Lading, J. Adin Mann, Jr., and R. V. Edwards, *J. Opt. Soc. Am.* A **6**, 1692 (1989).
4. H. L. Pécseli, *Electrostatic Drift Waves*, Lecture notes, University of Oslo.

### 2.2.3 Spectral analysis of plasma turbulence time series

*T. Jessen and P. K. Michelsen*

A hybrid Doppler/time-of-flight laser anemometer has recently been developed at Risø, and has been installed at the Wendelstein 7-AS stellarator. The experiment yields time series of the fluctuating plasma density at two neighbouring measurement volumes. The subsequent data analysis and interpretation have prompted the development and implementation of a new spectral data analysis technique.

The spectral analysis has been applied to model time series, obtained by numerically solving the Hasegawa-Mima equation for plasma drift wave turbulence as shown in Figure 7. Model data are useful for an initial test and verification of the basic mathematical machinery. Noise and other experimental effects can be added to the data and their influence on the analysis can be studied. In particular, the effect of scattering geometry (e.g. the size, shape, alignment and distance of

measurement volumes) in the actual experiment can be investigated. From the model simulation, time series *x(t), y(t)* of the plasma density at two probe positions are obtained. A preanalysis step involves decomposing each series into an ensemble of elementary series, weighted by a window function that minimises amplitude leakage. The data are subsequently fast Fourier transformed to frequency space, where the actual analysis is performed.

The cross-power spectrum and cross-correlation are first computed. The two-point correlation is used to estimate the time-of-flight of density fluctuations between the two probes and, hence, to estimate their typical propagation speed. A more refined correlation analysis, applied to each individual frequency component, yields the frequency-dependent phase velocity $w/k$ and thus the dispersion relation $k = k(w)$. In combination with the power spectrum we can then estimate the wave number spectrum. Therefore, the two-probe systems allows us to resolve and identify oscillations in both frequency and wave number space, and to find their interrelation.

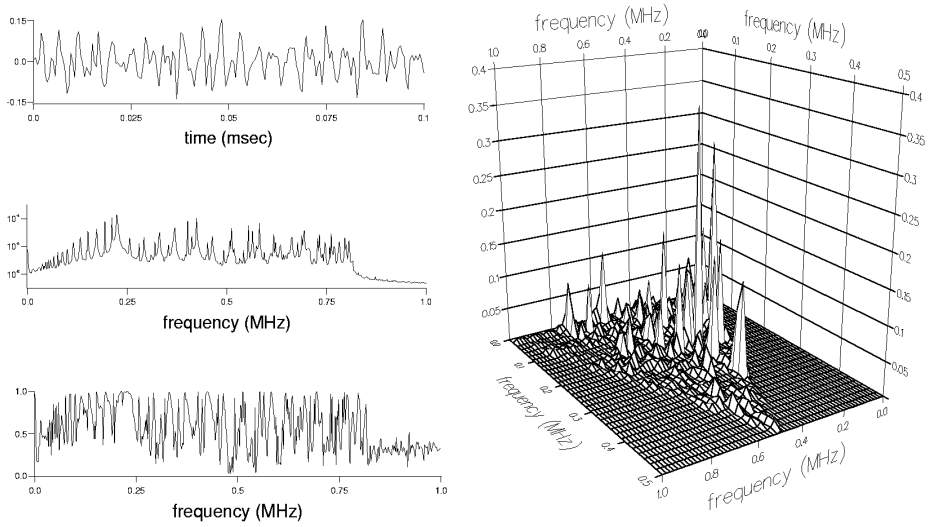


Figure 7. Example output of spectral time series analysis. The Hasegawa-Mima equation was solved to yield an ensemble of 256 plasma density time series to be analysed. Left (top): typical plasma density fluctuations, (middle) ensemble average power spectrum showing the presence of linear modes with minor peaks due to nonlinear wave coupling, (bottom) probe-pair coherence spectrum detects oscillations coherent over distances exceeding the probe separation to be included in the correlation analysis. Right: bicoherence spectrum reveals nonlinear wave triplet interactions at the dominant 200 kHz range.

Nonlinear wave dynamics is identified by bispectral analysis. The bispectrum directly measures the nonlinear coupling between wave triplets and vanishes for uncorrelated waves. It is found to be a useful indicator of nonlinear effects, by studying the transition from linear to strongly nonlinear wave dynamics in the Hasegawa-Mima model. Bispectral analysis can consequently detect and identify nonlinear effects

such as three-wave coupling, spectral cascades and formation of coherent structures.

The spectral techniques outlined here are now being employed in the analysis of W7-AS fluctuation data.

# 2.3 Nonlinear Dynamics of Fusion Plasmas

### 2.3.1 Full three-dimensional simulations of the Hasegawa-Wakatani model

*S. B. Korsholm and P. K. Michelsen*

Drift wave turbulence is believed to be a good explanation for the anomalous transport of particles out of a fusion plasma. A model describing these drift waves is the Hasegawa-Wakatani model. In this model the drift waves are linearly unstable and are driven by the density gradient at the edge of the plasma. The model is described by two partial differential equations in the perturbations of the density, $n$, and the electrostatic potential, $\phi$. The equations are coupled through a term of the form $\frac{\partial^2}{\partial z^2}(\phi - n)$, where $z$ is parallel to the magnetic field.

Previous simulations have been performed using this model in a two-dimensional geometry. Since it is assumed that the motion of the particles is only due to $\vec{E} \times \vec{B}$-drift (i.e. in a plane perpendicular to the magnetic field), this was believed to be a fairly good assumption. The coupling between the equations has thus been done under the assumption of only one significant wave to number, $k_z$. Recent simulations showed, however, that full three-dimensional solutions of the equations were necessary. A full three-dimensional code has now been developed using accurate spectral methods in a tripple periodic geometry, and an example of the results is shown in Figure 8. The resolution of the fields has naturally been smaller than in the two-dimensional case, but as many as 96×96×64 modes in the $x$-$y$-$z$-directions have been used. The difference from the two-dimensional case is significant. After an initial phase of exponential growth due to the linear instability, the system saturates into a quasi-stationary turbulent state. The total energy is nearly constant and is mainly transferred into the $k_z = 0$ mode. This corresponds to the formation of so-called convective cells. In the present model/geometry these reduce the particle flux. The convective cells are large coherent structures and are apparently formed irrespective of the initial conditions.

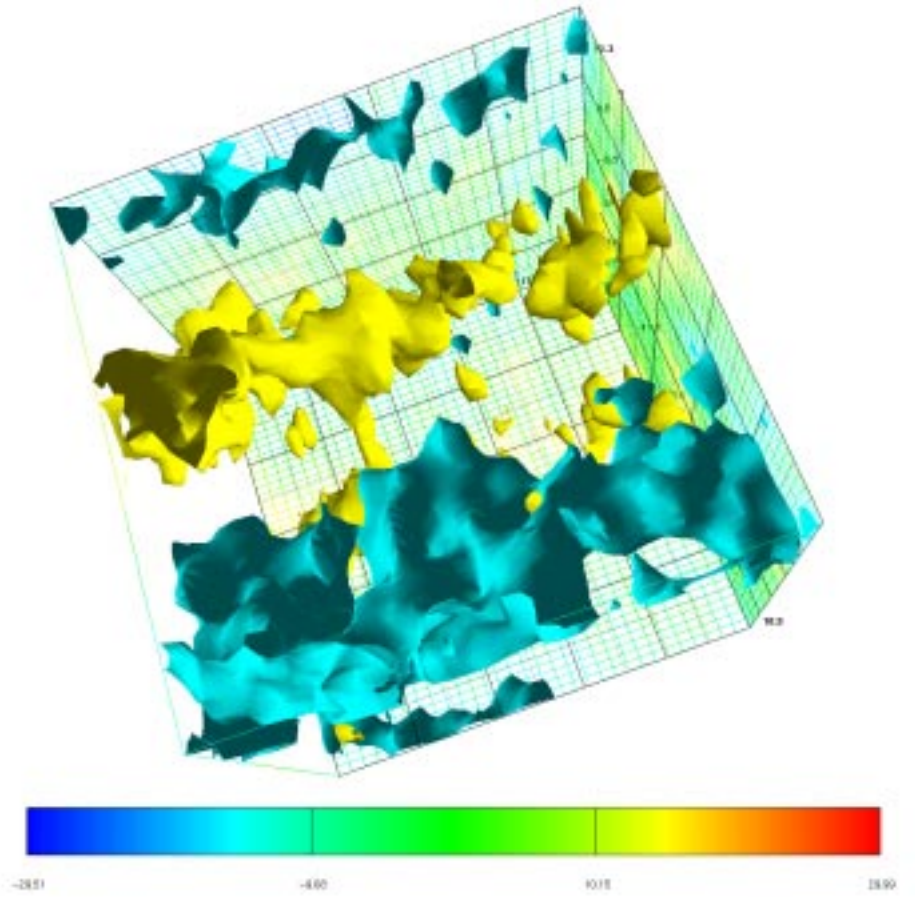

Figure 8. A plot of isosurfaces of the potential perturbation after saturation in the quasi-turbulent state. The simulation was started with low level noise as initial condition. The structures are parallel to the $z$-axis corresponding to very low $k_z$.

### 2.3.2 Numerical simulations of drift and flute modes in cylindrical and toroidal geometry

*V. Naulin, P. K. Michelsen, and S. B. Korsholm*

Most current numerical simulations of plasma turbulence do not consider the influence of boundaries onto the flow. However, the use of periodic boundary conditions makes it impossible to describe any backreaction of the turbulence onto the background quantities. The appearance of ballooning modes in the presence of magnetic curvature and the subsequent buildup of a poloidal shear flow, as shown for a two-dimensional simulation in Figure 9, is an example of a global mode, which reacts onto background quantities. For drift modes, a backreaction can only be described in a fully three-dimensional context. To approach this problem, whose understanding is crucial for the construction and design of fusion machines, effective numerical codes have to be developed. At present the necessary computational power is only available at reasonable cost through the use of parallel machines. Such a code has been developed for use on the IBM SP2. First results obtained for a fixed density profile, thus describing only fluctuating quantities have been obtained. The data produced by a system of equations

comparable to the well-known Hasegawa-Wakatani equations show that the dynamics change significantly with the imposed boundary conditions. The nonlinear polarisation drift produces a charge separation along the density background density gradient. By this, a poloidal shear flow (or counter-streaming) develops. This is a feature connected to the L-H transition in Tokamak machines. Figure 10 shows a typical result of one of these early simulations. In the ongoing project, the next step is to include in an appropriate way the magnetic field configuration of toroidal machines and by this to be able to perform fully nonlinear simulations including the dynamics of the background quantities.

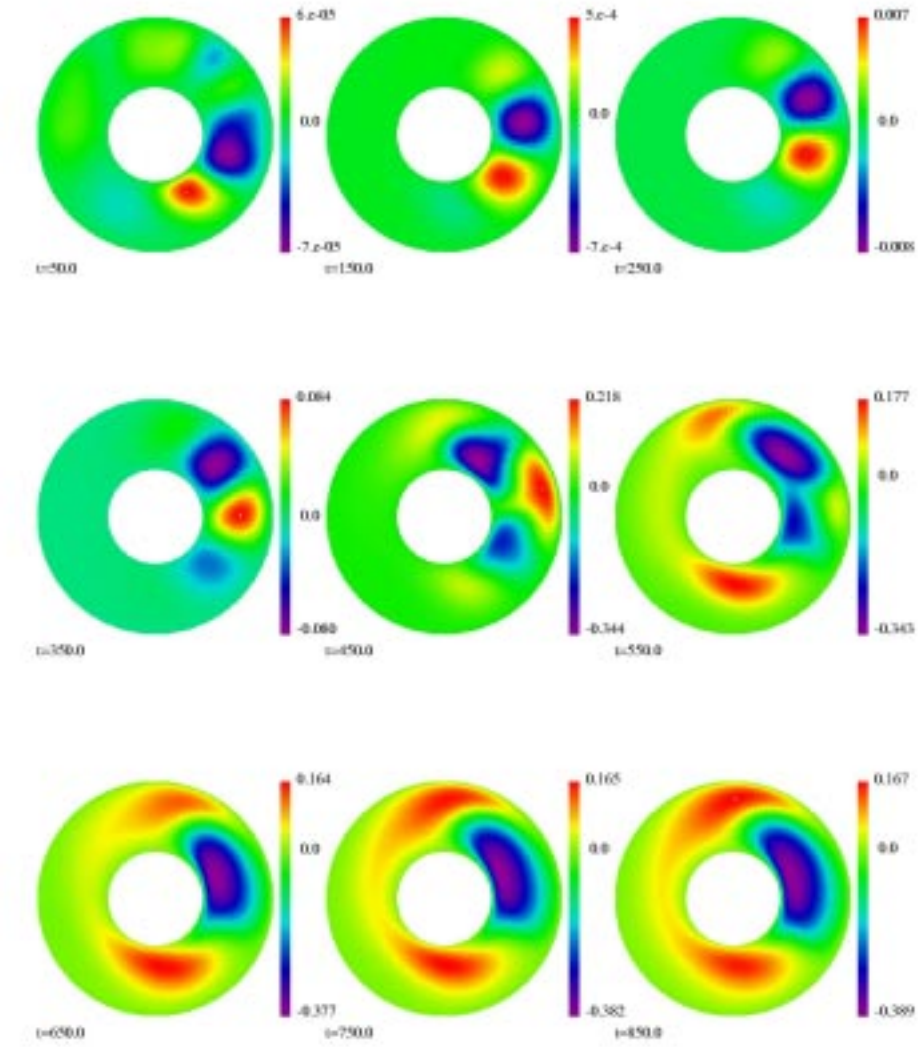

Figure 9. Development of ballooning modes and poloidal counter-streaming in the presence of magnetic curvature.

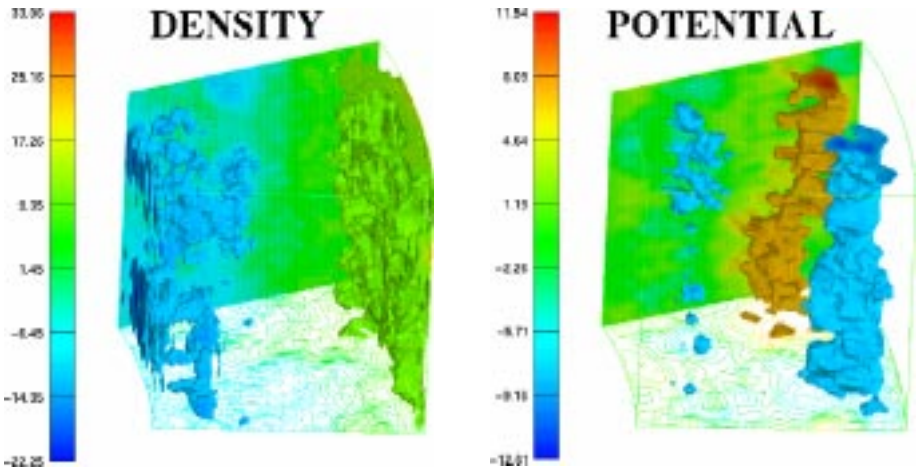


Figure 10. Density and potential fluctuations in a part of a cylindrical plasma.

### 2.3.3 Diffusion of ideal particles in electrostatic turbulence and the relation to coherent structures

*V. Naulin, A. H. Nielsen and J. J. Rasmussen*

The diffusion of particles in the presence of self-organised vortical structures, which are capable of trapping them, is a long-standing problem. Here we look at ideal particles in a 2D Model of electrostatic turbulence. The motion of charged particles in this situation is not only important for the understanding of the observed anomalous transport in fusion machines, but also for the diagnostic of fast alpha-particles leaving the reaction zone of a fusion device. Furthermore this problem is strongly connected to transport processes in the oceans and atmosphere. The reason for numerical simulations is that within this framework it is easy to distinguish between regions containing particles trapped in a vortical structure and regions with particles being convected by the fluctuating velocity field. While there are some simulations concerning particle diffusion in marginally disturbed static velocity fields, decaying turbulence, or a mixture of linear waves, we used turbulence driven by an internal instability to obtain the velocity field by which the ideal particles are convected. A large number of particles were followed through the flow using an accurate spectral scheme to evaluate the velocities at the particle positions. Furthermore it was evaluated if particles are within coherent structures at a time. Particles trapped in moving structures show a superdiffusion type in this type of turbulence, since the structures move in a non-random fashion. Simulations using more artificial velocity fields showed that nonlinear structures reduce the particle transport, since there is no motion of the structures themselves. For the free particles, we find normal diffusion setting in after a short ballistic phase. As the coherent structures only have a finite lifetime, there is a second ballistic time-scale after which the transport is again of the diffusion type. Recently[1] this type of “diffusion” has also been used to explain unexpectedly high concentrations achieved during mixing processes.

1. G. Vailati, *Nature* **390**, 262 (1997).

### 2.3.4 Models of dynamics of plasmas confined by curved magnetic fields

*K. Rypdal*, O. E. Garcia* (*University of Tromsø, Norway), V. Naulin and J. Juul Rasmussen*

Magnetically confined plasmas exhibit plasma turbulence with intermittent, large, coherent structures. While the modes with a vanishing parallel component are driven by, e.g., the interchange instability, which is due to magnetic field curvature and a density gradient, drift waves with parallel wave number different from zero are driven unstable by density and/or temperature gradients in combination with finite parallel resistivity. Models for flute modes as for resistive drift waves are well established. Here we are developing a three-field model that describes the evolution of the electrostatic potential, the plasma density and the electron temperature. As limiting cases the two simpler models mentioned above are included. Thus, we will be able to describe fluctuating quantities as well as the evolution of the background profiles. Moreover, by formulating this extended model, the range of validity of the various reduced models can be investigated. A proper reduction describing a given experimental set-up can then more easily be found.

A second problem one can only access with this kind of model, as it describes the plasma not only locally as the reduced models do but globally, is the investigation of the influence of boundary conditions on the plasma dynamics. Even though a vast amount of work has been performed as regards the evolution of sheets, the backreaction of the walls onto the plasma turbulence has not yet been considered in detail.

### 2.3.5 Anomalous cross-field current and fluctuating equilibrium of magnetised plasmas

*K. Rypdal*, O. E. Garcia* and J-V. Paulsen* (*University of Tromsø, Norway)*

Anomalous cross-field transport of mass and energy due to low frequency, electrostatic fluctuations is known to influence the formation of equilibria in magnetically confined plasmas. It has not been generally recognised, however, that anomalous cross-field current plays a similar role in some plasma discharges. By simple physical arguments and simulations based on a fluid model we have shown[1] that low frequency, electrostatic, flute-mode fluctuations can sustain a cross-field plasma current in addition to transport of mass and energy. The results show that this current determines essential features of the fluctuating plasma equilibrium, and explain qualitatively the experimental equilibria and the coherent flute-mode structure observed in a simple magnetised torus.

1. K. Rypdal, O.E. Garcia and J-V. Paulsen, *Phys. Rev. Lett*. **79**, 1857 (1997).

### 2.3.6 Turbulent equipartition and plasma transport

*V. Naulin, J. Nycander (FOA, Stockholm, Sweden) and*
*J. Juul Rasmussen*

Cross-field transport is one of the most important and most difficult areas of fusion research. Even basic transport phenomena, such as the L-H transition, the profile resilience and the particle pinch have no generally accepted explanations. Turbulent transport driven by low frequency electrostatic fluctuations is recognised to be of significant importance and may account for the major part of the transport in particular in the edge region of the plasma. Whereas classical collisional transport is generally down the gradients (of temperature and density) and tend to bring the plasma towards thermal equilibrium, turbulent transport may be directed up-gradient. This type of transport, which is directed inward from the edge of the plasma to the centre, leads to peaking of the density and temperature profiles and is referred to as the "pinch flux". Recently[1] it has been suggested that this inward transport can be explained by *Turbulent EquiPartition (TEP)*. This is based on the existence of Lagrangian invariants in the presence of the turbulence. The system relaxes towards equipartition of these quantities in the accessible phase space.

In order to test this equipartition hypothesis in a simplified system, we have derived a two-dimensional model describing the nonlinear evolution of pressure driven electrostatic flute modes in an inhomogeneous magnetic field. The model consists of a set of partial differential equations coupling fluctuations in density and electron temperature with the fluctuations in the electrostatic potential. Using a quasi-linear approach, we found that the turbulence driven by the Rayleigh-Taylor instability may give rise to a "pinch flux". Further, the conditions for marginal stability coincide with the profiles predicted by the turbulent equipartition[2].

The equations have been solved numerically on a two-dimensional domain bounded in the direction of the gradient of the magnetic field, and periodic in the other direction. We have investigated different ways of driving the system, e.g. with a localised temperature or a density source in the interior. In the cases investigated, we observe a clear pinch flux of both temperature and density and the saturated profiles tend to approach the profiles predicted from TEP.

In Figure 11 we show an example of the saturated temperature and density profiles for the case where the plasma is driven by keeping the left and right wall at a constant temperature. The inhomogeneity of the magnetic field is modelled using a linear dependence. Boundary conditions in the x-direction are that the temperature is fixed at both boundaries, while the density flux is set to zero at the boundaries. It is observed that the profiles are close to the ones predicted by the TEP; that is $n \approx B$ and $T \approx 2/3\ B$ holds in the centre region where turbulent mixing takes place. At both walls, a boundary layer can be seen where the flow is dominated by viscosity.

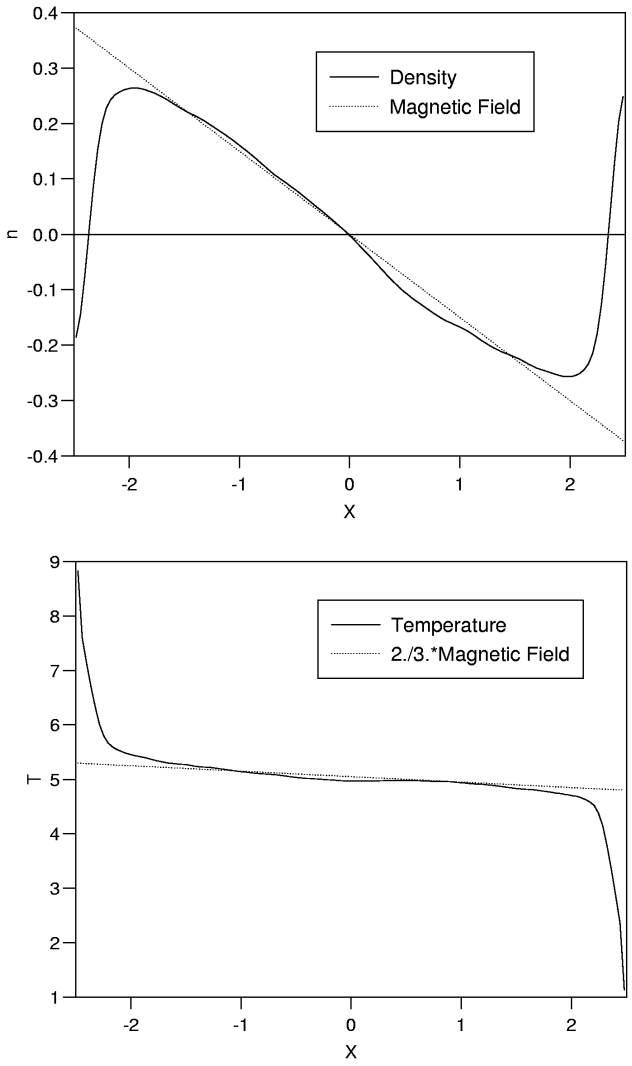


Figure 11. Time averaged profiles of density *n* and temperature *T* in the case where the plasma is driven by heating at one and cooling at the other wall.

1. V.V. Yankov and J. Nycander, *Phys. Plasmas* **4**, 2907 (1997).
2. J. Nycander and J. Juul Rasmussen, *Plasma Phys. Control. Fusion* **39**, 1861 (1997).

### 2.3.7 Model of cold pulse propagation with sign inversion in tokamaks

*V. K. Mezentsev (Institute for Automation and Electrometry, Novosibirsk, Russia), J. Juul Rasmussen and V. V. Yankov (RRC Kurchatov Institute, Moscow, Russia)*

The phenomenon of cold pulse propagation with sign inversion is a well-known example of anomalous behaviour of transport in tokamak plasmas.[1] In these experiments the plasma response to local cooling of the plasma electrons near the edge of the tokamak was investigated. The temperature pulse was observed to propagate very rapidly through the edge region of the plasma and the temperature increased promptly in the inner third part of the plasma column. Thus, a cold heat pulse propagates inwards and inverses its sign as it approaches the centre of the column.

This effect can certainly not be modelled by standard transport models. In these models the transport can be expressed as the sum of the products of transport coefficients and thermodynamic forces related to the gradients of density and temperature, where the coefficients are functions of the local thermodynamic variables as density and temperature. The phenomenon was simulated numerically[1] by an ad hoc introduced variation of thermal conductivity with radius.

We have suggested a transport model that is based on the idea that turbulent transport drives the plasma towards a state of Turbulent EquiPartition (TEP).[2] This state appears as the relaxed state in which Lagrangian invariants that are not destroyed by the turbulence are uniformly distributed. We have thus expanded the fluxes near the TEP state, and by solving the obtained transport equation we reproduce the cold pulse propagation and the sign inversion. It should be emphasised, that the aim is not to construct a predictive transport model, but rather to demonstrate the essential importance of the underlying physical model. Here, the main ingredient is the non-local response of the effective turbulent diffusion coefficient and its relation to the marginally stable profiles of temperature and density, the TEP state.

1. K. W. Gentle et al., *Phys. Rev. Lett*. **74**, 3620, (1995); *Phys. Plasmas* **4**, 3599 (1997).
2. V. V. Yankov and J. Nycander, *Phys. Plasmas* 4, 2907 (1997).

### 2.3.8 Multidomain pseudospectral scheme for full-wave calculations in complex geometries

*P. G. Dinesen, J. S. Hesthaven (Brown University, USA) and J. P. Lynov*

A usual assumption in many calculations of electromagnetic wave propagation in inhomogeneous plasmas is that the 'local' wavelength of the electromagnetic wave is much shorter than the characteristic scale length of the plasma inhomogeneity. However, this 'WKB' or 'geometric optics' assumption is often violated in cases of practical interest connected to heating or diagnostics of plasmas. When the WKB assumption breaks down, a full-wave solution of Maxwell's equations is needed. This is normally a very difficult task due to the complex geometries in practical problems.

Recently, a new and efficient method[1] for the accurate determination of electromagnetic scattering from conducting objects with complex geometries has been developed. This method is based on a multidomain pseudospectral scheme, which is well suited for implementation on parallel supercomputers. We are presently adopting this method to the solution of problems of electromagnetic wave propagation in inhomogeneous dielectrics with characteristic scale lengths similar to, or even smaller than, the free-space wavelength.

1. B. Yang, D. Gottlieb, and J. S. Hesthaven, *J. Comput. Phys*. **134**, 216 (1997).

### 2.3.9 Ion temperature gradient vortices in shear flow

*P. K. Michelsen, J. Juul Rasmussen and N. Chakrabati (Institute of Plasma Physics, Bhat, India)*

Recent tokamak experiments have shown improved stability and confinement properties in plasma regions with high velocity shear. A sheared plasma flow caused by an inhomogeneous perpendicular electric field may have strong influence on the generation and evolution of vortical structures. The shear field may tear the structures apart and may result in smaller scales of the coherent structures, thereby limiting their contribution to the transport.

To investigate the influence of velocity shear on coherent structures we have studied the evolution of monopolar and dipolar vortices in an ITG-model. The equations were solved numerically by a spectral method in a two-dimensional domain with periodic boundary conditions. Monopoles or dipoles are used as initial condition superimposed on the shear field. The dipoles used are stationary solutions to the equations without shear.

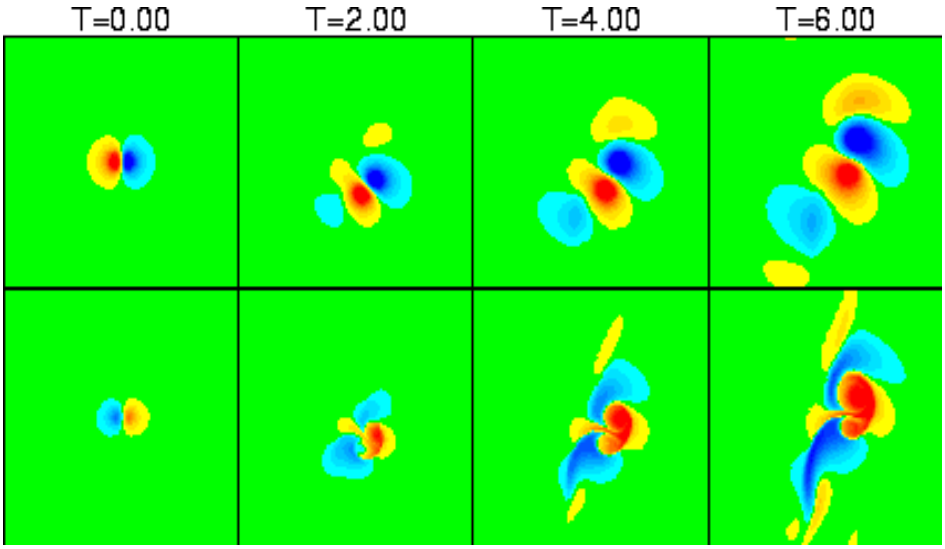


Figure 12. The evolution of the potential (upper row) and the pressure (lower row) versus time.

In Figure 12 the evolution of the potential (upper row) and the pressure (lower row) versus time is shown. A dipole is initialised in a strong shear field, but in a region where the mean velocity is zero. By its own vorticity field it starts moving in the negative *y*-direction, but it is slowly turning around because of the shear field and it moves into the region where the background velocity is in the *y*-direction. Therefore, the dipole eventually moves in the *y*-direction. Although the dipole itself keeps together, new vortices of opposite sign are created where the positive one becomes the strongest. At this stage the total structure resembles a tripole. Theoretical investigations have indicated that tripoles could be stationary solutions to the equations including velocity shear. For a case where the initial condition consists of a row of monopoles

close together in the *y*-direction, vortices of opposite sign are created between the monopoles. These new vortices are stretched out between the original monopoles by the vorticity field and a row of new monopoles is created on each side. The row of original monopoles located along the line of maximum shear seems to be rather stable for a long time. However, investigations of single monopoles have shown that they are normally very unstable in the shear field.

### 2.3.10 Equilibrium and movement of ideal MHD plasmas in magnetic fields

*V. O. Jensen*

A detailed study of the physics governing ideal MHD plasmas which are acted upon by external forces and confined in magnetic fields has been initiated. It is shown that some of the arguments commonly used to explain the physics of how equilibrium is obtained are not giving the most intuitive insight. It is further shown that the concept of magnetic stresses and the equations of ideal MHD together constitute a good basis for a physical understanding of the interaction between plasmas and magnetic fields.

## 2.4 External Projects

### 2.4.1 Pellet Injectors

*P.K. Michelsen, B. Sass, and J. Bundgaard (Engineering and Computer Department)*

During 1997, consultant assistance on pellet injectors has been given in two instances. In the beginning of the year, B. Sass and J. Bundgaard visited Frascati in order to discuss the possibility of inserting the two stage driver from the Italian high speed single shot pellet injector in one port of the eight-shot Risø made pellet injector.

Later in the year, help was given to Frascati and Culham in connection with the modification and installation of the pellet injector on START. This pellet injector was originally built at Risø for ETA-BETA in Padova more than 10 years ago.

### 2.4.2 Laser anemometry for power-curve measurement and control of wind turbines

*L. Lading and S. Frandsen (Wind Energy and Atmospheric Physics Department)*

The work on plasma turbulence measurements is based on the use of $CO_2$ lasers, detection and spectral measurements by light beating, as well as components for the far infrared part of the optical spectrum. A spin-off from this work has materialised in work on laser anemometers for wind turbines. The laser anemometry work is based on the same general concepts as the work on plasma diagnostics. A patent application was submitted early 1997 and has now been updated. A collaborative effort

with two Danish companies and one British company has been established. Contract negotiations with the Commission about a project on this topic under the *Joule* programme are in the final state. Without the general knowledge established through the Euratom Association and in particular the diagnostics work for the W7-AS stellarator at IPP Garching it would have been very difficult for Risø to enter the long-range laser anemometry field.

## 2.5 Participants in Fusion Plasma Physics

**Scientific Staff**

Jensen, Vagn O.
Lynov, Jens-Peter
Michelsen, Poul K.
Nielsen, Anders H.
Rasmussen, Jens Juul
Saffman, Mark

**Post Docs**

Dinesen, Palle G. (from 1 October)
Naulin, Volker
Svendsen, Winnie E.

**Ph.D. Students**

Jessen, Thomas
Schmidt, Michel R.

**Technical Staff**

Astradsson, Lone
Bækmark, Lars
Reher, Børge (until 31 July)
Sass, Bjarne
Thorsen, Jess

**Guest Scientists**

Garcia, Odd Eric, University of Tromsø, Norway
Hesthaven, Jan, Brown University, Rhode Island, USA
Mezentsev, Vladimir, Institute of Automation and Electrometry, Russian Academy of Sciences, Novosibirsk, Russia
Paulsen, Finn-Victor, University of Tromsø, Norway
Rypdal, Kristoffer, University of Tromsø, Norway

**Short-term Visitors**
Chakrabarti, Nikhil, Institute of Plasma Research, Bhat, India
Pécseli, H.L., University of Oslo, Norway
Wyller, John, Narvik Institute of Technology, Norway
Yankov, V.V., Russian Research Center Kurchatov Institute, Moscow, Russia

**Students Working for the Master's Degree**

Heinemeyer, Nicholas
Korsholm, Søren Bang

**Student Assistants**

Pécseli, Thomas

# 2.6 Publications

### 2.6.1 International Publications

Hesthaven, J.S.; Juul Rasmussen, J.; Berge, L.; Wyller, J., Numerical studies of localized wavefields governed by the Raman-extended derivative nonlinear Schrödinger equation. J. Phys. A (1997) v. 30 p. 8207-8224.

Lading, L.; Saffman, M.; Edwards, R.V., Laser anemometry based on collective scattering: the effects of propagating and nonpropagating fluctuations. Opt. Lasers Eng. (1997) v. 27 p. 531-542.

Nielsen, A.H.; Juul Rasmussen, J., Formation and temporal evolution of the Lamb-dipole. Phys. Fluids (1997) v. 9 p. 982-991.

Nycander, J.; Juul Rasmussen, J., Pinch effect in two-dimensional turbulence. Plasma Phys. Control. Fusion (1997) v. 39 p. 1861-1869.

Rypdal, K.; Garcia, O.E.; Paulsen, J.V., Anomalous cross-field current and fluctuating equilibrium of magnetized plasmas. Phys. Rev. Lett. (1997) v. 79 p. 1857-1860.

Svanstedt, N.; Wellander, N.; Wyller, J., A numerical algorithm for nonlinear parabolic equations with highly oscillating coefficients. Numer. Methods Partial Differential Equations (1996) v. 12 p. 423-440.

### 2.6.2 Conference Lectures

Michelsen, P.K.; Sunn Pedersen, T.; Juul Rasmussen, J., Numerical studies of drift wave turbulence. In: Theory of fusion plasmas. Proceedings. Joint Varenna-Lausanne international workshop on theory of fusion plasmas, Varenna (IT), 26-30 Aug 1996. Connor, J.W.; Sindoni, E.; Vaclavik, J. (eds.), (Editrice Compositori, Bologna, 1997) p. 505-510.

Michelsen, P.K.; Sunn Pedersen, T.; Juul Rasmussen, J., Lyapunov exponents and particle dispersion in drift-wave turbulence. In: Proceedings of the 1996 international conference on plasma physics. Vol. 1. ICCP 96, Nagoya (JP), 9-13 Sep 1996. Sugai, H.; Hayashi, T. (eds.), (Japan Society of Plasma Science and Nuclear Fusion Research, Nagoya, 1997) p. 914-917.

Michelsen, P.K.; Sunn Pedersen, T.; Juul Rasmussen, J., Resistive coupling in drift wave plasma turbulence. In: Proceedings of the 1996 international conference on plasma physics. Vol. 1. ICCP 96, Nagoya (JP), 9-13 Sep 1996. Sugai, H.; Hayashi, T. (eds.), (Japan Society of

Plasma Science and Nuclear Fusion Research, Nagoya, 1997) p. 918-925.
Naulin, V.; Spatschek, K.H., Contribution of coherent structures in drift-wave turbulence to particle transport. In: Supercomputation in nonlinear and disordered systems. Algorithms, applications and architectures. Euroconference on supercomputation in nonlinear and disordered systems, Madrid (ES), 23-28 Sep 1996. Vázquez, L.; Tirado, F.; Martín, I. (eds.), (World Scientific Publishing Co., Singapore, 1997) p. 373-374

### 2.6.3 Publications for a Broader Readership

Jensen, V.O., Fusionsenergi. In Danmarks Nationalleksikon, Den Store Danske Encyklopædi. (1997) v. 7, p. 196-198.
Jensen, V.O., Hybridreaktor. In Danmarks Nationalleksikon, Den Store Danske Encyklopædi. (1997) v. 8, p. 122.
Jensen, V.O., International Thermonuclear Reaktor. In Danmarks Nationalleksikon, Den Store Danske Encyklopædi. (1997) v. 8, p. 436.
Jensen, V.O., Inertifusion. In Danmarks Nationalleksikon, Den Store Danske Encyklopædi. (1997) v. 8, p.372.
Svendsen, W.; Saffman, M., Målinger af tæthedsfluktuationer i et fusionsplasma. DOPS-Nyt (1997) v. 12 (no.4) p. 14-18.

### 2.6.4 Unpublished Lectures

Garcia, O.E.; Rypdal, K., Numerical simulation of plasma in a simply magnetized torus. 32. Nordic plasma and gas discharge symposium, Longyearbyen (NO), 2-5 Mar 1997. Unpublished. Abstract available.
Jensen, V.O., Comment on the equilibrium of toroidal plasmas. 32. Nordic plasma and gas discharge symposium, Longyearbyen (NO), 2-5 Mar 1997. Unpublished.
Jensen, V.O., Fusion plasma physics. 28 lectures at the Technical University of Denmark, Lyngby (DK), Jan - Dec 1997. Unpublished.
Jensen, V.O., Introduction to the course fusion plasma physics. Course on fusion plasma physics, Lyngby (DK), 2 May 1997. Unpublished.
Jessen, T.; Michelsen, P.K.; Saffman, M.; Svendsen, W., Analysis of collective light scattering in terms of drift wave turbulence models. In: The 7th European fusion theory conference. Programme and abstracts. 7. European fusion theory conference, Jülich (DE), 8-10 Oct 1997. Forschungszentrum Jülich, Jülich, 1997) Paper P1-7.
Juul Rasmussen, J., Self-organization and vortex structures. Nonlinear science day, Danish Ph.D. School in Nonlinear Science, Risø (DK), 19 Nov 1997. Unpublished.
Michelsen, P.K., Numerical simulation of two-dimensional resistive drift wave turbulence. Leopold-Franzenz Universität Innsbruck, Innsbruck (AT), 29 Apr 1997. Unpublished.
Michelsen, P.K., Vortex dynamics, Lyapunov exponents and particle dispersion in drift wave turbulence. Leopold-Franzenz Universität Innsbruck, Innsbruck (AT), 5 May 1997. Unpublished.
Michelsen, P.K.; Juul Rasmussen, J.; Chakrabati, N., Ion temperature gradient vortices in shear flow. In: The 7th European fusion theory

conference. Programme and abstracts. 7. European fusion theory conference, Jülich (DE), 8-10 Oct 1997. (Forschungszentrum Jülich, Jülich, 1997) Paper P1-3.

Naulin, V., Structure detection in drift-wave turbulence. IUTAM symposium on simulation and identification of organized structures in flows. Technical University of Denmark, Lyngby (DK), 25-29 May 1997. Unpublished. Abstract available.

Naulin, V., Structures an transport in driftwave turbulence. 32. Nordic plasma and gas discharge symposium, Longyearbyen (NO), 2-5 Mar 1997. Unpublished. Abstract available.

Naulin, V., Detection of coherent structures in driftwave turbulence. Symposium on two-dimensional turbulence in plasmas and fluids, Canberra (AU), 16 Jun - 11 Jul 1997. Unpublished. Abstract available.

Naulin, V., Structures and transport in drift-wave turbulence. In: The 7th European fusion theory conference. Programme and abstracts. 7. European fusion theory conference, Jülich (DE), 8-10 Oct 1997. (Forschungszentrum Jülich, Jülich, 1997) Paper O-4.

Naulin, V., Numerical simulation of drift and flute modes in cylindrical geometry. In: The 7th European fusion theory conference. Programme and abstracts. 7. European fusion theory conference, Jülich (DE), 8-10 Oct 1997. (Forschungszentrum Jülich, Jülich, 1997) Paper P1-4.

Naulin, V., Numerical investigation on global and local effects of structures in a 2D-flow-model on particle transport. Transport processes in the atmosphere and the oceans. TAO working group meeting on coherent structures and transport, Risø (DK), 29 Oct - 1 Nov 1997. Unpublished. Abstract available.

Naulin, V., Diffusion of ideal particles in a 2D model of electrostatic turbulence. Workshop on stochastic transport theory, Bruxelles (BE), 2-3 Dec 1997. Unpublished. Abstract available.

Nielsen, A.H., Temporal evolution of the Lamb-Dipole. Koninklijk Nederlands Meteorologisch Instituut (KNMI), Utrecht (NL), 21 Nov 1997. Unpublished.

Nielsen, A.H., Particle transport across a circular shear layer with coherent structures. FOM-Institute voor Plasmafysica Rijnhuizen, Nieuwegein, Utrecht (NL), 24 Nov 1997. Unpublished.

Nielsen, A.H.; Lynov, J.P.; Juul Rasmussen, J., Particle transport across a circular shear layer with coherent structures. In: The 7$^{th}$ European fusion theory conference. Programme and abstracts. 7th European fusion theory conference, Jülich (DE), 8-10 Oct 1997. (Forschungszentrum Jülich, Jülich, 1997) Paper P1-24.

Rasmussen, J. Juul, Transport and coherent structures. In: The 7$^{th}$ European fusion theory conference. Programme and abstracts. 7. European fusion theory conference, Jülich (DE), 8-10 Oct 1997. (Forschungszentrum Jülich, Jülich, 1997) Paper I-3.

Rasmussen, J. Juul; Konijnenberg, J. van de; Nielsen, A.H.; Stenum, B., Shear flow instability and vortex dynamics. 32. Nordic plasma and gas discharge symposium, Longyearbyen (NO), 2-5 Mar 1997. Unpublished.

Rypdal, K., Anomalous cross-field currents in magnetized plasma. 32. Nordic plasma and gas discharge symposium, Longyearbyen (NO), 2-5 Mar 1997. Unpublished. Abstract available.

Rypdal, K.; Garcia, O.E.; Paulsen, J.-V., Anomalous currents in laboratory and space plasmas. IPELS 97, Maui, HI (US), 23-27 Jun 1997. Unpublished. Abstract available.

Svendsen, W., $CO_2$ laser scattering experiment at W7-AS. Seminar at Institute of Plasma Physics, Garching (DE), 15 Aug 1997. Unpublished.

Svendsen, W.; Saffman, M.; Sass, B., Measurements of density fluctuations in a fusion plasma using $CO_2$ laser scattering. In: Danish Physical Society annual meeting 1997. Programme. Annual meeting of the Danish Physical Society, Nyborg (DK), 23-24 May 1997. (HCØ Tryk, København, 1997) p. AP21P.

# 3. Fusion Technology

## 3.1 Introduction

The work reported in this section has been carried out in the Materials Research Department. The overall objective of the research activities in this area is to determine the impact of neutron irradiation on physical and mechanical properties of metals and alloys, so that appropriate materials can be chosen for their application in an irradiation environment (e.g. in a fusion reactor). Various experimental techniques are employed to study different aspects of the microstructural evolution during irradiation and the resulting consequences on the post-irradiation physical and mechanical properties of metals and alloys. Computer simulations are carried out to understand the evolution of surviving defects and their clusters in collision cascades. The kinetics of defect accumulation during irradiation and the influence of irradiation-induced defects and their clusters on the deformation behaviour of irradiated metals and alloys are studied theoretically. In the following, the main results of these activities are highlighted.

## 3.2 Next Step Technology (ITER Task T213/EU)

### 3.2.1 Effect of Bonding and Bakeout Thermal Cycles and Neutron Irradiation on Physical and Mechanical Properties of Copper Alloys

*B.N. Singh, D.J. Edwards *, M. Eldrup and P. Toft (*Pacific Northwest National Laboratory, USA)*

Precipitation and dispersion strengthened copper alloys (CuCrZr, CuNiBe, and Glid Cop CuAl-25) are being considered as heat sink materials in the first wall and divertor assemblies of ITER because of their high thermal conductivity and relatively high strength. Several irradiation experiments have shown that each of these alloys will impose severe restrictions upon the designers due to their susceptibility to radiation hardening and concomitant loss of ductility, work hardening and fracture toughness. It has been also recognized that the joining procedures employed in fabricating the components will also affect the performance of the materials during irradiation since the optimal heat treatments needed to achieve the desired thermal conductivity and strength may not be realized during the industrial manufacturing processes.

As part of a broad experimental study of the effects of heat treatments and subsequent irradiation on the properties of these candidate alloys, a series of heat treatments were given to tensile specimens of CuCrZr, CuNiBe and CuAl-25 alloys. These heat treatments were chosen to

simulate the effects of bakeout treatments and possible joining treatments such as isostatic pressing. These specimens were then irradiated in the DR-3 reactor at Risø at 50, 100, 250 and 350$^{o}$C to a dose level of ~0.3 dpa. The results of the irradiation experiments conducted at ~50, 250 and 350$^{o}$C have been reported earlier. In the following, the results of the finial set of screening experiments on the same materials irradiated to ~0.3 dpa at 100$^{o}$C are summarized.

The effects of various heat treatments on the unirradiated microstructure have been reported earlier and will not be repeated here. Tensile properties of unirradiated and irradiated specimens of different alloys with various heat treatments tested at 100$^{o}$C are described. The results of electrical resistivity measurements at 23$^{o}$C are also reported.

The materials used in these experiments were CuCrZr, CuNiBe and CuAl-25 alloys. The CuCrZr and CuNiBe alloys were supplied by Tréfimétaux (France) in the form of 20 mm thick plates. The dispersion strengthened CuAl-25 alloy was supplied by OGM Americas (formerly SCM Metals Inc.) in the form of rods in the as-extruded (i.e. wrought) condition. The chemical composition of these alloys is given in Table 1. For the screening experiments, the tensile specimens of CuCrZr and CuNiBe alloys were given five different heat treatments (A, B, E, C and C[1]) and are described in Table 2. The bonding thermal heat treatment for CuAl-25 specimens consisted of annealing at 950$^{o}$C for 30 min. (referred to as heat treatment D). All heat treatments were carried out in vacuum (<$10^{-5}$ torr). Tensile specimens of copper alloys with different heat treatments were irradiated in the DR-3 reactor at Risø at 100$^{o}$C to a fast neutron fluence level of 1.5 x $10^{24}$ n/m$^{2}$ (E > 1 MeV), which corresponds to a displacement dose of ~0.3 dpa (NRT).

| | |
|---|---|
| OFHC-Cu: | Cu - 10, 3, < 1 and < 1 ppm of Ag, Si, Fe and Mg, respectively |
| CuCrZr: | Cu - 0.8% Cr, 0.07% Zr, 0.01% Si |
| CuNiBe: | Cu - 1.75% Ni, 0.45% Be |
| CuAl25 | Cu - 0.25% Al as oxide particles (0.46% $Al_2O_3$) |

Table 1: Chemical Composition of the Copper and Copper Alloys

| Type | Heat Treatment |
|---|---|
| A | Solution annealing at $950^0$C for 1 h followed by water quench |
| E | Prime ageing: heat treatment A + ageing at $475^0$C for 30 min. followed by water quench |
| B | Bonding thermal cycle: heat treatments A + E + annealing at $950^0$C for 30 min. followed by furnace cooling + re-ageing at $475^0$C for 30 min. followed by furnace cooling |
| C | Bakeout thermal cycle: heat treatment B + annealing at $350^0$C for 100 h followed by furnace cooling |
| C' | Bakeout thermal cycle: heat treatment E + annealing at $350^0$C for 100 h followed by furnace cooling |
| D | Annealing at $950^0$ C for 30 min. (only for CuAl-25) |
| D' | CuAl-25 in the as-wrought condition, i.e. without any heat treatment |

Table 2: Summary of bonding and bakeout heat treatments for CuCrZr, CuNiBe and CuAl alloys

Both unirradiated and irradiated tensile specimens were tested in an INSTRON machine at a strain rate of $1.2 \times 10^{-3}$ $s^{-1}$. Tensile tests were carried out $100^o$C in vacuum (>$10^{-5}$ torr). The test temperature of $100^o$C was reached within 30 min. All resistivity measurements were made at room temperature ($23^o$C), using a 4-point probe module developed at Risø. The resistivity was normalized to that of pure copper and converted to electrical conductivity.

For transmission electron microscopy (TEM), 3 mm discs were punched from the unirradiated and irradiated tensile specimens and thinned mechanically down to ~0.1 mm thickness. These discs were then twin-jet electropolished in a solution of 25% perchloric acid, 25% ethanol and 50% water at 11V for about 15 seconds at ~$20^o$C. Specimens were examined in a JEOL 2000 FX transmission electron microscope.

The irradiation-induced defect microstructure as well as changes in the precipitate size and density were quantitatively characterized using TEM investigations. The cluster density in the irradiated CuCrZr specimens was found to be ~$5.6 \times 10^{23}$ $m^{-3}$, independent of the heat treatment given prior to irradiation. The size distributions of the stacking fault tetrahedra (SFT) were virtually the same in all specimens and yielded an average size of 2.3 nm for the SFTs. The density of precipitate in the CuCrZr specimens after irradiation was found to be ~$2.6 \times 10^{22}$ $m^{-3}$, slightly lower than the values of ~$3.6 - 5.9 \times 10^{22}$ $m^{-3}$ measured in the unirradiated specimens. The average size of the precipitates measured in the irradiated specimens ranged from 4.5 to 5.6 nm, roughly double of the size measured in unirradiated specimens. A relatively low density of dislocation loops and segments were also observed in the irradiated CuCrZr specimens. No precipitate denuded zones were observed along the grain boundaries in either the unirradiated or the irradiated specimens.

The microstructure of the CuNiBe alloys revealed that these alloys are not as stable against irradiation as the CuCrZr alloys. The density of

precipitates in the unirradiated specimens with the prime ageing (E) and bonding thermal cycle (B) heat treatments ranged from 14 to 18 x $10^{23}$ $m^{-3}$, respectively. After irradiation the precipitate density in the heat treated E and B specimens, respectively, decreased to 4.0 and 5.5 x $10^{23}$ $m^{-3}$. The precipitate size in these alloys was also affected by irradiation. The size of the γ‘ precipitates in unirradiated specimens was found to be 3.8 nm for the prime-aged specimens and 6.6 nm for the specimens with the bonding thermal cycle heat treatment. After irradiation, the average precipitate size in both types of specimens was found to be ~3 nm. Irradiation at 100°C leads to precipitation within the pre-irradiation precipitate denuded zones and also in the grain boundary itself. These precipitates appear to the same as the γ‘ precipitates in the matrix.

Resistivity measurements made before and after irradiation revealed that microstructural changes induced by irradiation also led to a measurable effect on the physical properties of these alloys. Table 3 lists the electrical conductivity (normalised to OFHC-Cu) measured before and after irradiation at 100°C. The decrease in conductivity in the irradiated OFHC-Cu and CuAl-25 is due to transmutation products and defect clusters produced during irradiation. The increase in the conductivity in the CuCrZr alloy, on the other hand, is most probably due to irradiation-induced transport of Cr and Zr atoms from the matrix to the existing precipitates. This would be consistent with the TEM observation that the precipitates in CuCrZr grow in size during irradiation. There is no obvious explanation for the decrease in the conductivity observed in CuCrZr specimen with the heat treatment C. The fact that the conductivity of CuNiBe specimens decreases due to irradiation supports the interpretation that the precipitates in these specimens suffer from ballistic dissolution. The fact that the conductivity of CuNiBe specimen with heat treatment B reaches a low value of ~38% only after a displacement dose of 0.3 dpa would suggest that the application of CuNiBe alloys in a strong irradiation environment is not an attractive proposition.

| Material | Heat Treatment | Unirradiated | Irradiated |
|---|---|---|---|
| OFHC | 550°C/2 h | 100 | 88.4 |
| CuNiBe | A | 33.7 | 31.3 |
| CuNiBe | E | 48.8 | 41.4 |
| CuNiBe | B | 49.3 | 37.7 |
| CuNiBe | Hycon 3HP | 64.6 | 54.6 |
| CuCrZr | A | 47.9 | 55.1 |
| CuCrZr | E | 52.3 | 61.2 |
| CuCrZr | B | 59.5 | 72.4 |
| CuCrZr | C | 78.8 | 66.3 |
| CuAl-25 | D | 89.2 | 80.3 |

Table 3. Electrical conductivity for Copper Alloys Irradiated at 100°C to a Dose Level of 0.3 dpa

Tensile results for the unirradiated and irradiated specimens of different alloys irradiated at 100°C are quoted in Tables 4 and 5. The stress-strain curves for specimens tested at 100°C are shown in Figures 1-3 for CuCrZr, CuNiBe and CuAl-25 alloys, respectively. These results show that the tensile strength of the unirradiated CuCrZr alloy is sensitive to heat treatments whereas various heat treatments do not seem to affect the tensile properties of the unirradiated CuNiBe alloys. As can be seen from Figure 1 the tensile behaviour of the CuCrZr alloy is also very sensitive to neutron irradiation at 100°C. All irradiated CuCrZr specimens, irrespective of their pre-irradiation heat treatment, show yield drop, strong plastic instability, no work hardening and a drastic decrease in the uniform plastic elongation. In other words, the CuCrZr alloy irradiated at 100°C is unable to deform plastically in a homogeneous fashion. The CuNiBe and CuAl-25 alloys also suffer from a drastic reduction in their uniform elongation and work hardening ability, but do not exhibit the kind of plastic instability as CuCrZr does.

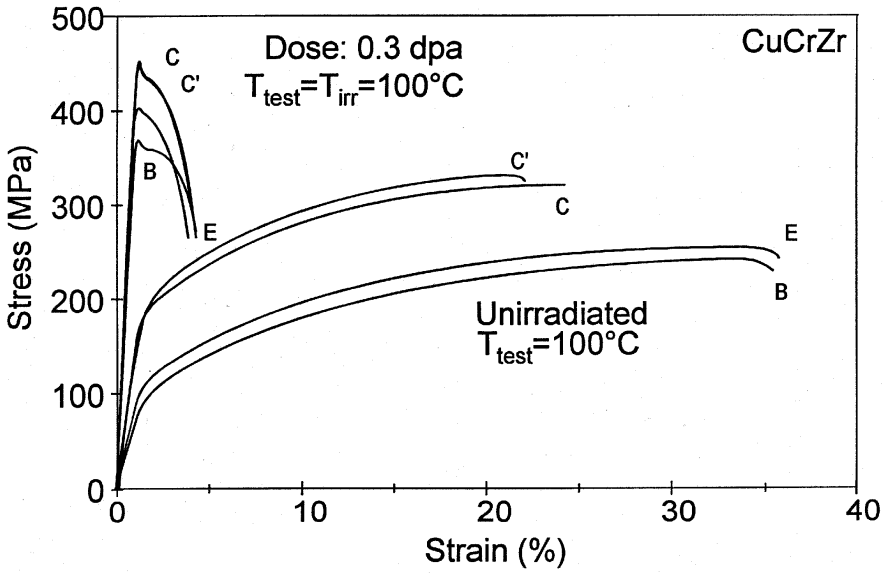


Figure 1. Stress-strain curves for the unirradiated and irradiated CuCrZr alloy with different pre-irradiation heat treatments (see Table 2). Note the loss of uniform elongation due to irradiation.

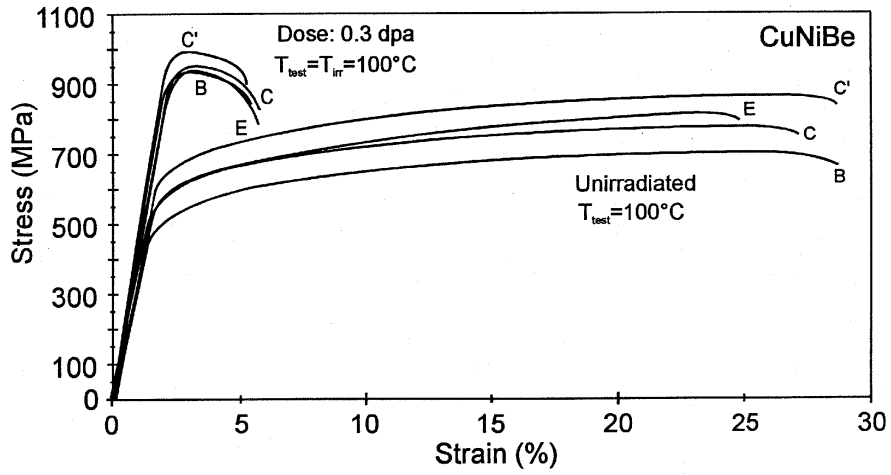


Figure 2. Stress-strain curves for the unirradiated and irradiated CuNiBe alloy with different pre-irradiation heat treatments (see Table 2). Note the reduction in ductility due to irradiation.

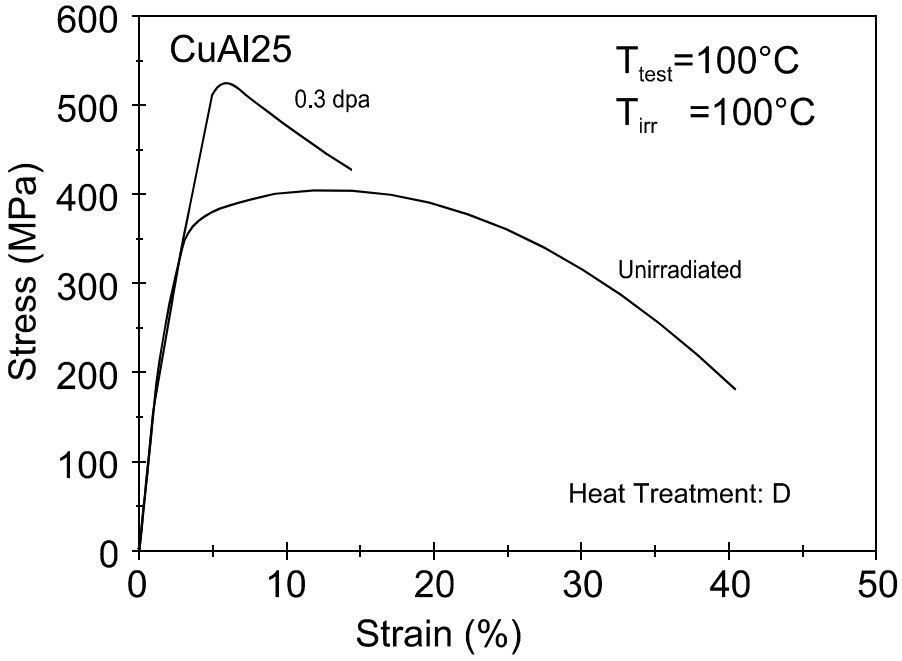


Figure 3. Stress-strain curves for the unirradiated and irradiated CuAl-25 alloy. Note the reduction in ductility due to irradiation.

| Material | Heat-Treatment | $\sigma_{0.05}$ (MPa) | $\sigma_{0.2}$ (MPa) | $\sigma_{max}$ (MPa) | $\varepsilon^{p}_{u}$ (%) | $\varepsilon_{total}$ (%) |
|---|---|---|---|---|---|---|
| OFHC-Cu | 550°C/2 h | 20 | 26 | 193 | 60.0 | 64.0 |
| CuNiBe | A | 103 | 108 | 340 | 55.0 | 58.0 |
| CuNiBe | B | 450 | 470 | 690 | 28.0 | 30.0 |
| CuNiBe | C | 530 | 555 | 760 | 25.5 | 27.5 |
| CuNiBe | C' | 600 | 630 | 860 | 27.0 | 28.0 |
| CuNiBe | E | 550 | 580 | 820 | 24.0 | 25.0 |
| CuNiBe | Hycon 3HP | - | 720 | 780 | 7.2 | 11.4 |
| CuCrZr | A | 65 | 70 | 205 | 43.0 | 44.0 |
| CuCrZr | B | 94 | 99 | 237 | 34.8 | 36.2 |
| CuCrZr | C[a] | 170 | 180 | 315 | - | - |
| CuCrZr | C' | 175 | 185 | 322 | 23.0 | 24.3 |
| CuCrZr | E | 105 | 110 | 246 | 34.0 | 35.5 |
| CuAl-25 | D[b)] | 340 | 355 | 400 | 13.0 | 40.0 |

Table 4. Tensile Results for Unirradiated Pure OFHC-Cu and Copper Alloys with the Pre-irradiation Heat Treatments described in Table 2. Tests were conducted at 100°C.
[a)] Broke prematurely
[b)] Round specimen, 3 mm diameter gage

| Material | Heat-Treatment | $\sigma_{0.05}$ (MPa) | $\sigma_{0.2}$ (MPa) | $\sigma_{max}$ (MPa) | $\varepsilon^{p}_{u}$ (%) | $\varepsilon_{total}$ (%) |
|---|---|---|---|---|---|---|
| CuNiBe | A | 625 | 663 | 683 | 12.5 | 14.5 |
| CuNiBe | B | 800 | 880 | 938 | 3.4 | 5.9 |
| CuNiBe | C | 880 | 960 | 990 | 3.4 | 5.4 |
| CuNiBe | E | 815 | 885 | 940 | 3.3 | 5.9 |
| CuNiBe | Hycon 3HP | - | 810 | 840 | 0.8 | 4.5 |
| CuCrZr | A | 365 | 365 | 370 | 1.1 | 4.0 |
| CuCrZr | B | 370 | 370 | 373 | 1.1 | 4.1 |
| CuCrZr | C | 445 | 450 | 450 | 1.3 | 4.0 |
| CuCrZr | C’ | 440 | 440 | 445 | 1.3 | 4.0 |
| CuCrZr | E | 400 | 405 | 412 | 1.2 | 3.8 |
| CuAl-25 | D[b)] | 540 | 544 | 546 | 5.5 | 26.0 |

Table 5. Tensile Results for Copper Alloys Irradiated at 100°C to 0.3 dpa with Different Heat Treatments
[a)] Specimen broke prematurely
[b)] Round specimens, 3 mm diameter gage

### 3.2.2 Post-irradiation Annealing Effects

*B.N. Singh, M. Eldrup and P. Toft*

As shown in the preceding section, all three candidate copper alloys suffer a severe loss of ductility due to irradiation with neutrons at 100°C already at a dose level of 0.3 dpa. In principle, annealing of these irradiated specimens at and above the recovery stage V may cause annihilation of defect clusters responsible for the hardening and loss of ductility and thereby may improve the ductility.

To test out this possibility, a number of tensile specimens of CuCrZr, CuNiBe and CuAl-25 were irradiated at 100°C to displacement doses of 0.2 and 0.3 dpa. Tensile properties and electrical resistivity of these specimens were determined in the unirradiated, irradiated and irradiated and annealed (at 300°C for 50h in vacuum) conditions. The effects of post-irradiation annealing on the electrical conductivity and tensile

properties of the CuCrZr alloy were reported last year. Figure 4 and 5 show the effect of post-irradiation annealing on the tensile behaviour of CuNiBe and CuAl-25 alloys, respectively.

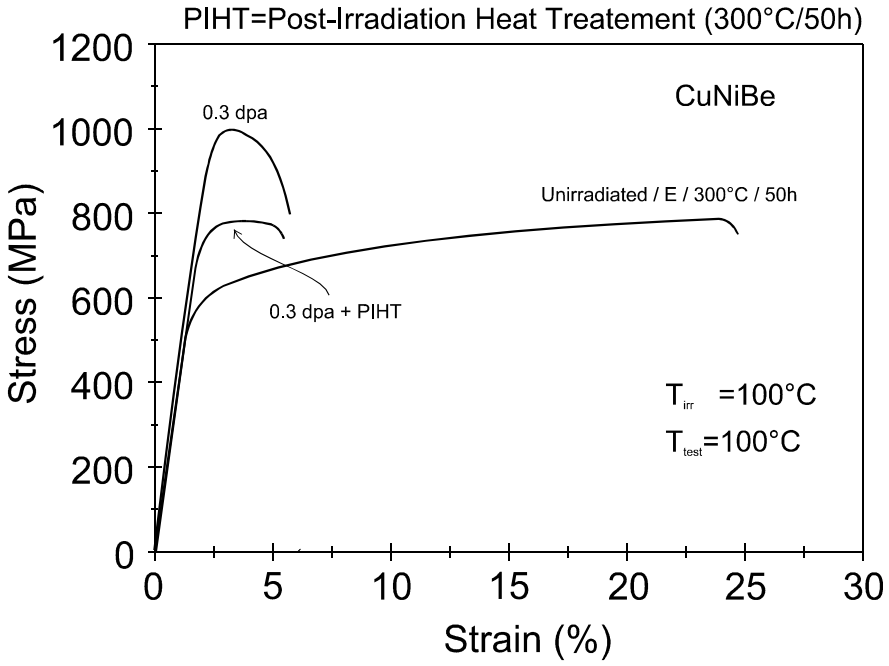


Figure 4. The effect of post-irradiation annealing (300°C/50 h) on the deformation behaviour of CuNiBe alloy with the pre-irradiation heat treatment E (Table 2) irradiated at 100°C. Note the improvement in the ductility due to the post-irradiation annealing.

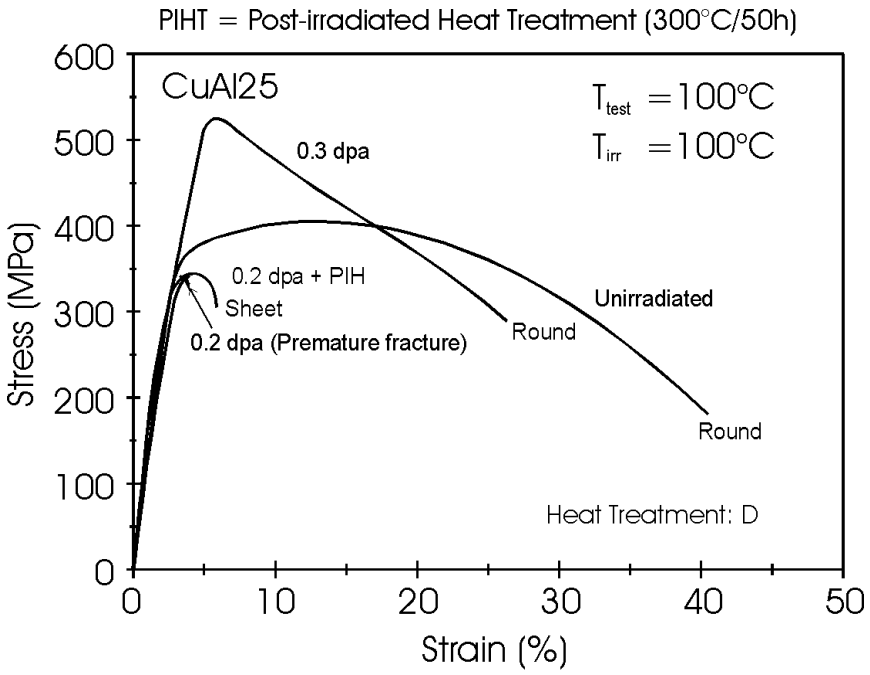


Figure 5. Same as Fig. 4 but for the CuAl-25 alloy irradiated at 100°C. Note a slight improvement in ductility due to post-irradiation annealing.

As expected, the post-irradiation annealing does cause a noticeable decrease in the yield stress compared to that in the as-irradiated condition. However, it is clear that the annealing at 300°C for 50 h does not lead to a full recovery. From the point of view of an improvement in the ductility of these alloys, the post-irradiation annealing eliminates the problem of yield drop and plastic instability and provides a few percent of uniform elongation. However, it should be noted that only a small fraction of the uniform elongation (compared to that of unirradiated specimens) is recovered after post-irradiation annealing. Furthermore, at the moment it is not clear whether or not even this recovery will be maintained under the condition of repeated irradiation and annealing.

### 3.2.3 Effect of Neutron Irradiation on Tensile and Fracture Toughness Behaviour of Copper Alloys

*S. Tähtinen*, M. Pyykkönen*, P. Karjalainen-Roikonen**
*(VTT Manufacturing Technology, Finland), B.N. Singh and P. Toft*

One of the most important factors in deciding about the applicability of copper alloys in the structural components of ITER is the effect of neutron irradiation on the fracture toughness behaviour of these alloys. Unfortunately, practically nothing has been reported in the open literature on the effect of irradiation on the fracture toughness properties of these copper alloys. Recently, a collaborative programme has been initiated between Risø National Laboratory and VTT Manufacturing Technology to investigate the effect of neutron irradiation on tensile as well as fracture toughness properties of CuAl-25 (IGO) and CuCrZr (Outokumpu) alloys.

The CuAl-25 (IGO) refers to Glid Cop CuAl-25 in cross rolled condition with a final heat treatment (D) at 980°C for 2 h; IGO stands for "ITER grade Zero". The material was supplied by OMG Americas (former SCM Metals Inc.) in the form of 20 mm thick plate. The CuCrZr alloy used in these investigations was supplied by Outokumpu OY (Finland) with main alloying elements Cr (0.78 wt.%) and Zr (0.13 wt.%). The material was supplied in the form of 40 mm thick place in hot-rolled condition. The plate was heat treated (F) at 960°C for 1 h followed by water quench and then aged at 460°C for two hours followed by air cooling.

Both tensile (0.3 mm thick) and single edge bend SE (B) fracture toughness specimens of dimensions 3 x 4 x 27 $mm^3$ were machined. Both tensile and fracture toughness specimens of CuCrZr (Outokumpu) and CuAl-25 (IGO) were irradiated with fission neutrons in the DR-3 reactor at Risø at 200 and 350°C to a dose level of 0.3 dpa (NRT). Irradiations were performed in the high temperature rig where irradiation temperature was monitored, controlled and recorded continuously throughout the whole irradiation period.

Both unirradiated and irradiated specimens of CuCrZr (Outokumpu) and CuAl-25 (IGO) were tested in an Instron machine (at Risø) at a strain rate of 1.2 x $10^{-3}$ $s^{-1}$ in a vacuum of ~$10^{-5}$ torr. Fracture resistance curves were determined (at VTT) using the displacement controlled three-point bend testing with a constant displacement rate of 1.5 x $10^{-2}$ mm/min.

Load, displacement and crack length (measured using the DC-PD method) were recorded during the testing and the fracture resistance curves were determined following the ASTM 1737 standard procedure.

The tensile results for both unirradiated and irradiated CuCrZr (F) and CuAl-25 (IGO) are shown in Figure 6 and 7, respectively. It should be noted that even at the irradiation temperature of 200°C (which is very close to or just above the recovery stage V for pure copper) both alloys show plastic instability. At the irradiation temperature of 350°C, on the other hand, both alloys show normal deformation behaviour. It is interesting to note here that at this temperature, the CuCrZr (F) alloy is somewhat stronger and considerably more ductile (after irradiation) than CuAl-25 (IGO).

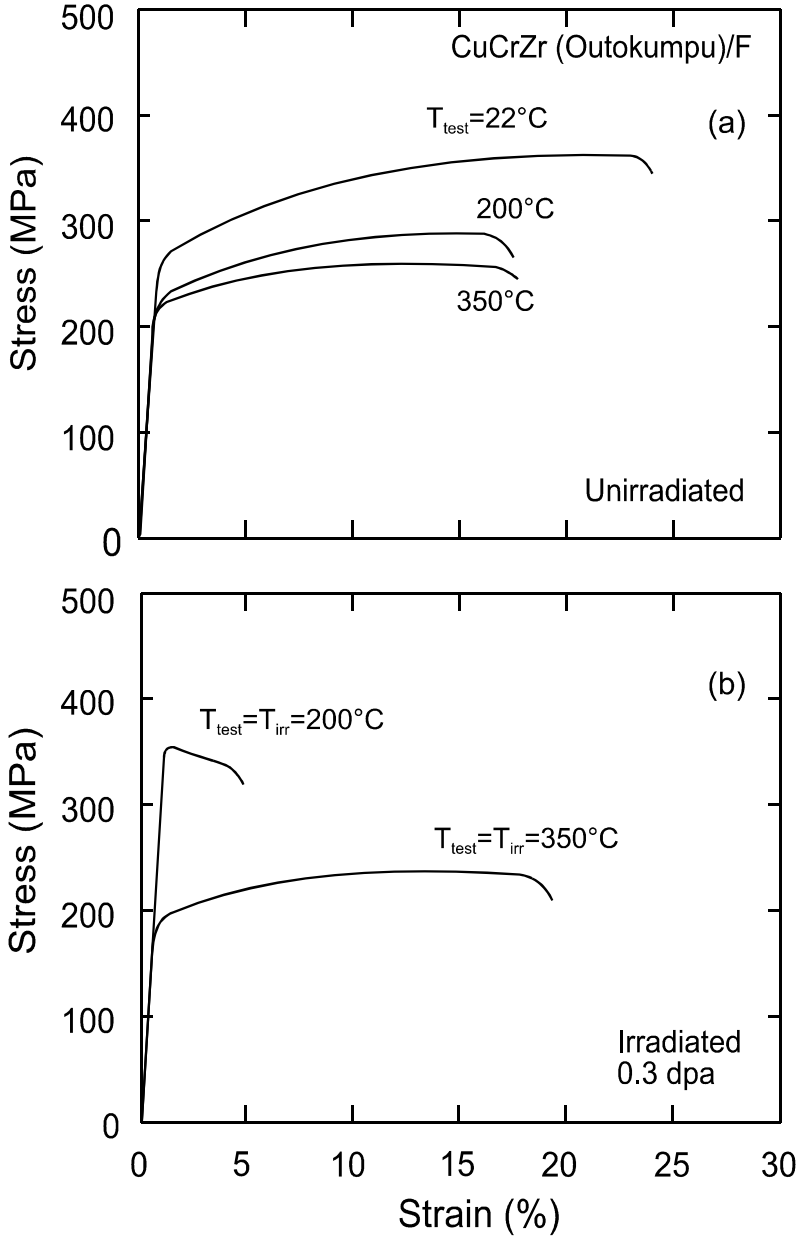


Figure 6. Stress-strain curves for the unirradiated and irradiated CuCrZr (Outokumpu) alloy. Note that the irradiation even at 200°C causes a complete loss of uniform elongation.

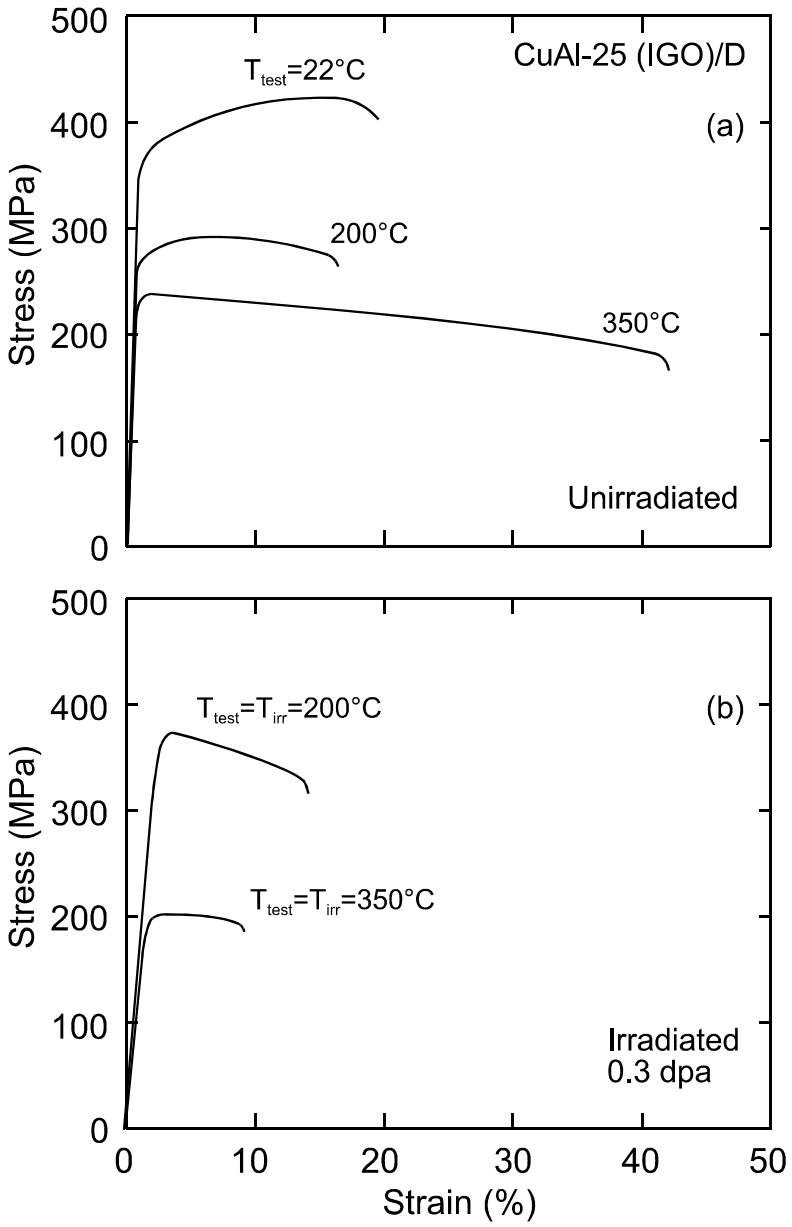


Fig. 7. The same as Fig. 6 but for CuAl-25 (IGO). Note the loss of uniform elongation due to irradiation at 200°C.

The fracture resistance curves were obtained for CuCrZr (F) and CuAl-25 (IGO) alloys as a function of test temperature. The CuAl-25 (IGO) alloy exhibited stable crack growth at all temperatures, whereas in CuCrZr (F) alloy extensive crack tip blunting occurred and stable crack growth was observed only at 350°C. Both the irradiation fracture toughness for stable crack growth and tearing resistance values were higher for CuCrZr (F) alloy than that for CuAl-25 (IGO).

The effect of neutron irradiation on the initiation fracture toughness of CuCrZr (F) and CuAl-25 (IGO) is shown in Figure 8 and 9, respectively, for temperatures up to 350°C. It can be seen that the fracture toughness decreases with increasing temperature in both alloys but the decrease is more rapid in the case of CuAl-25 (IGO). Furthermore, the fracture

toughness of CuAl-25 (IGO) is substantially lower than that of CuCrZr (F) at all temperatures. The results also demonstrate that the fracture toughness is considerably more sensitive to irradiation in the case of CuAl-25 (IGO) than in the case of CuCrZr (F) alloy. It is interesting to note that although the tensile elongation of CuCrZr (F) at 350°C is about the same both in the unirradiated and irradiated states, yet the fracture toughness in the irradiated CuCrZr (F) is found to be significantly lower than that in the case of unirradiated CuCrZr (F) alloy. At present, there is no clear explanation for this effect.

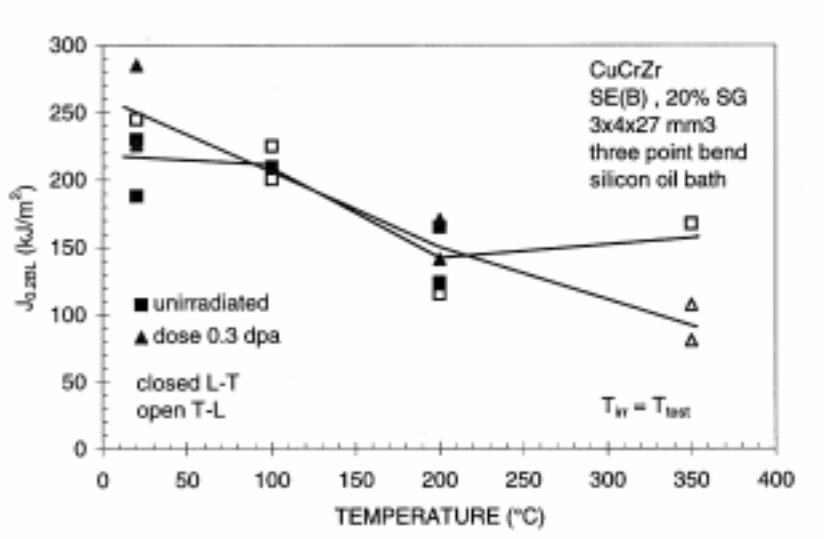


Figure 8. Effect of neutron irradiation (0.3 dpa) on the initiation fracture toughness $J_{0.2BL}$ of CuCrZr (Outokumpu) alloy. Note that the irradiation causes no significant decrease in the fracture toughness up to the irradiation temperature of 200°C. There is no clear explanation for the decrease observed at 350°C.

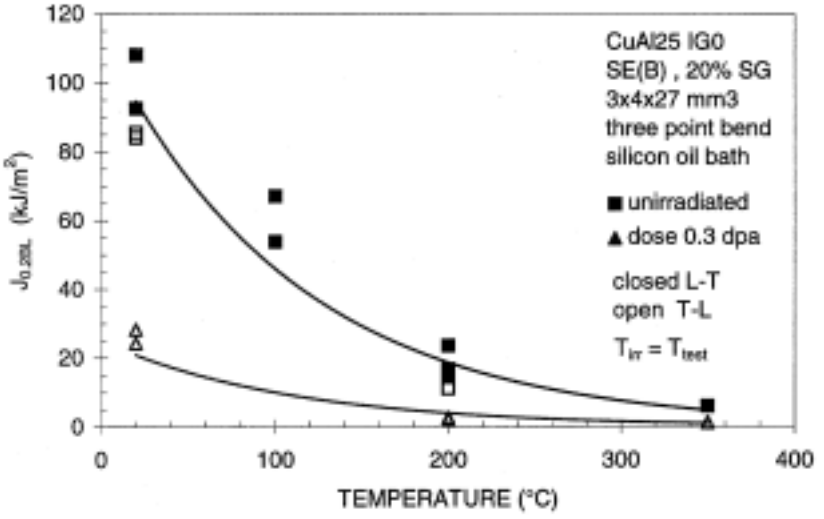


Figure 9. Effect of neutron irradiation (0.3 dpa) on the initiation fracture toughness $J_{0.2BL}$ of CuAl-25 (IGO) alloy. Note the lack of fracture toughness even in the unirradiated condition. The irradiation causes a drastic decrease in the fracture toughness, particularly at lower temperatures.

# 3.3 Long-Term Technology

### 3.3.1 Effects of Neutron Irradiation on Microstructure and Mechanical Properties of Iron and Low Activation Steels

*B.N. Singh, A. Horsewell and P. Toft*

Effects of neutron irradiation on physical and mechanical properties of low activation ferritic-martensitic steels are being extensively studied internationally since these alloys are considered to be candidate materials for the blanket and first wall of fusion reactors (e.g. DEMO and Commercial). Although these alloys are very resistant to void swelling and maintain good fracture toughness at irradiation temperatures above about 400°C, they are prone to loss of ductility at lower irradiation temperatures. This is a matter of serious concern from the point of view of mechanical performance and lifetime of these alloys under fusion irradiation conditions, particularly when the mechanism controlling the loss of ductility is not understood. The present work is a part of the European activities devoted to mechanistic studies of irradiation hardening and loss of ductility.

Tensile specimens of pure iron (annealed at 650°C for 2 h) were irradiated to different dose levels at 50°C between ~0.01 to ~0.4 dpa, at 100°C between ~$10^{-2}$ to ~0.2 dpa, and at 250°C to doses of ~0.1 and ~0.2 dpa. Additional specimens were irradiated at 200 and 350°C to a dose level of ~0.2 dpa. Tensile specimens of the modified F82H and MANET-2 specimens were irradiated at 100, 200, 250 and 350°C to a dose level of ~0.2 dpa. The irradiation of the F82H and MANET-2 specimens at 50°C is in progress now.

All irradiated specimens of pure iron have been tensile tested at the respective irradiation temperatures of 50, 100, 200, 250 and 350°C in vacuum (~$10^{-5}$ torr) at a strain rate of 1.3 x $10^{-3}$ $s^{-1}$. Specimens of F82H and MANET-2 irradiated at 250 and 350°C have been tensile tested in vacuum (~$10^{-5}$ torr) at the irradiation temperatures. Transmission electron microscopy (TEM) investigations have been carried out on pure iron specimens irradiated at 50°C in the as-irradiated and irradiated and deformed conditions. The fracture surfaces of both unirradiated and irradiated specimens were examined in a scanning electron microscope (SEM).

The variation of the irradiation-induced cluster density with the displacement dose is shown in Figure 10. Figure 10 also includes the results for the iron specimen irradiated at 250°C to ~0.2 dpa. It is interesting to note that the cluster density in pure iron is considerably lower than that in pure copper irradiated at a similar temperature and to similar dose levels.

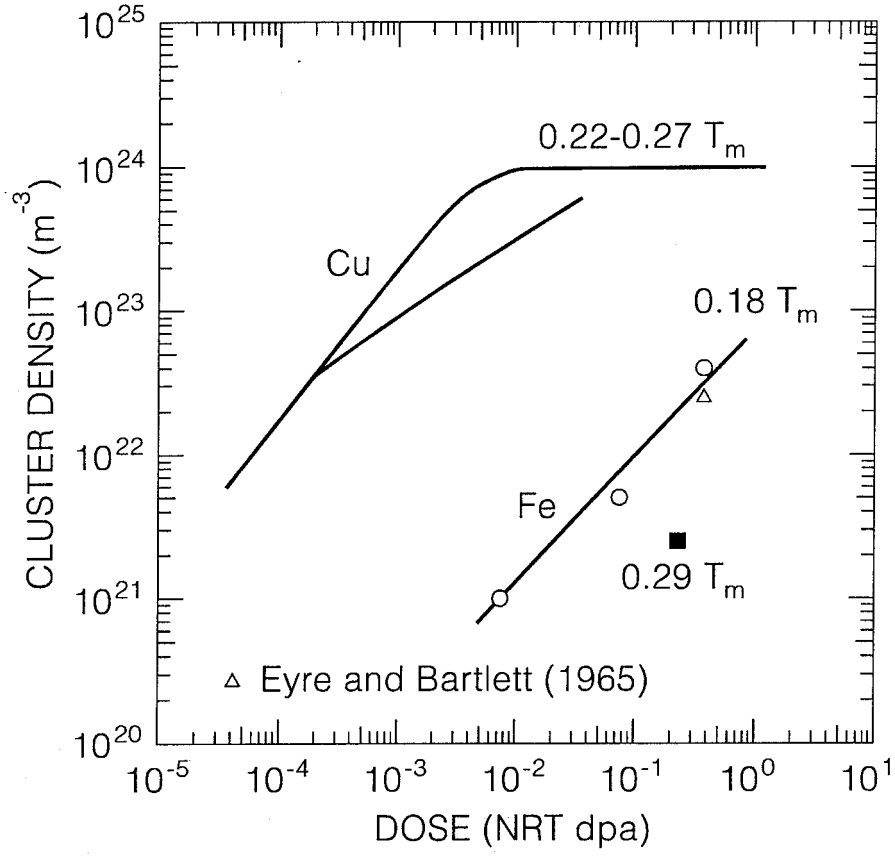


Figure 10. Dose dependence of cluster density in pure iron irradiated at 50°C. For comparison, results for pure copper are also shown.

The TEM investigation of specimens irradiated to ~0.4 dpa and deformed at ~50°C revealed an interesting and significant fact that the plastic deformation in these specimens occurs in a localized fashion and seems to be concentrated mainly in narrow deformation bands known as "cleared" channels (Figure 11 a). Meeting of these cleared channels at grain boundaries, surfaces and other cleared channels may lead to crack nucleation at these sites and may be responsible for causing brittle fracture (Figure 11b).

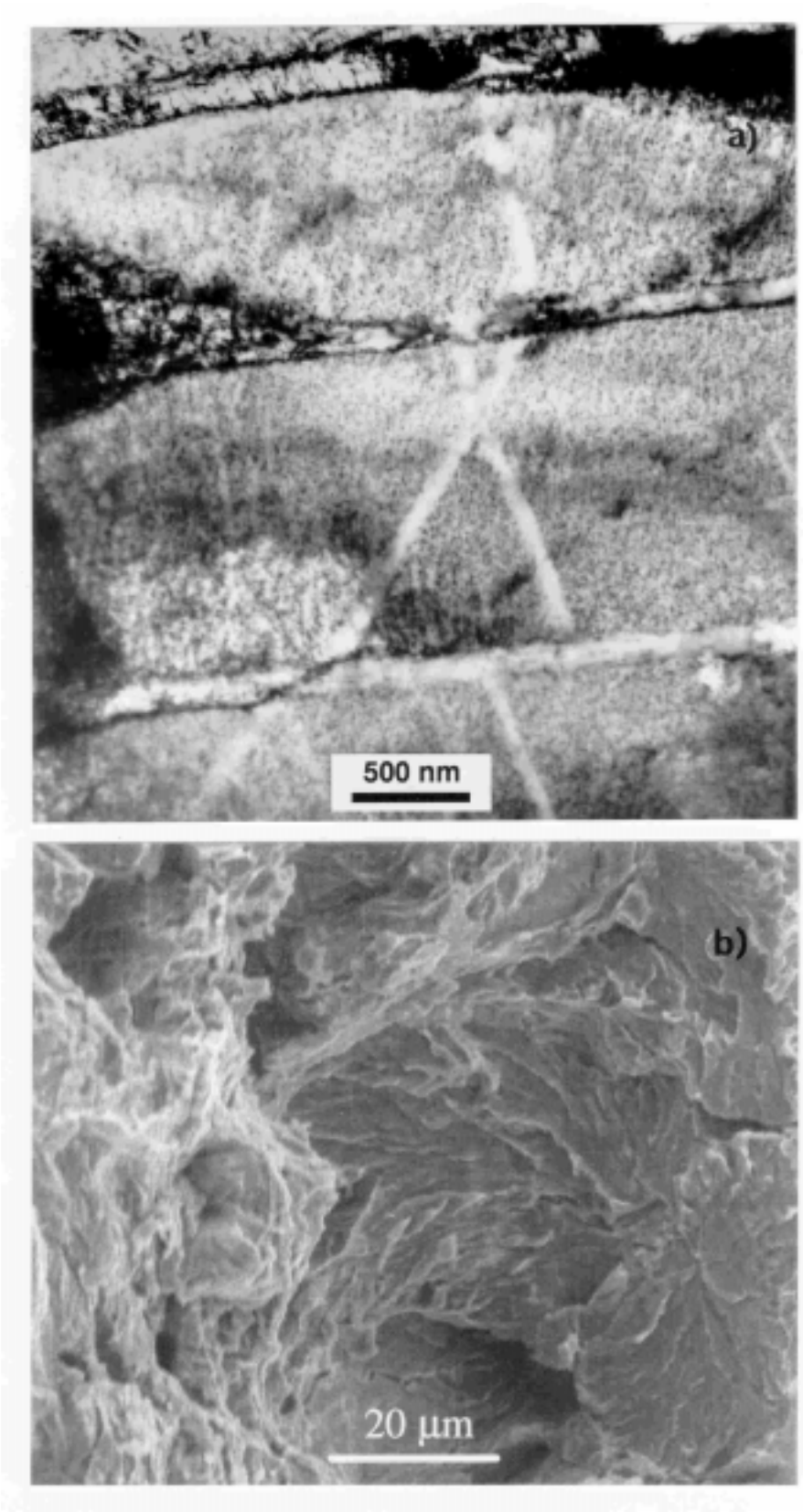


Figure 11. TEM micrograph showing (a) “cleared” channels and SEM fractographs showing (b) intergranular cleavage fracture in pure iron irradiated at 50$^{o}$C to a dose level of ~0.4 dpa (NRT). The specimen was tensile tested at 50$^{o}$C in vacuum (<$10^{-5}$ torr).

Figure 12 shows the stress-strain curves for pure iron irradiated at 100°C to different dose levels and tensile tested at 100°C (in vacuum of $<10^{-5}$ torr). For comparison, the stress-strain curve for the unirradiated reference specimen is also shown. Both the upper yield stress and the yield-drop increases with increasing dose level, whereas the work hardening decreases with the dose and becomes practically zero at the highest dose level.

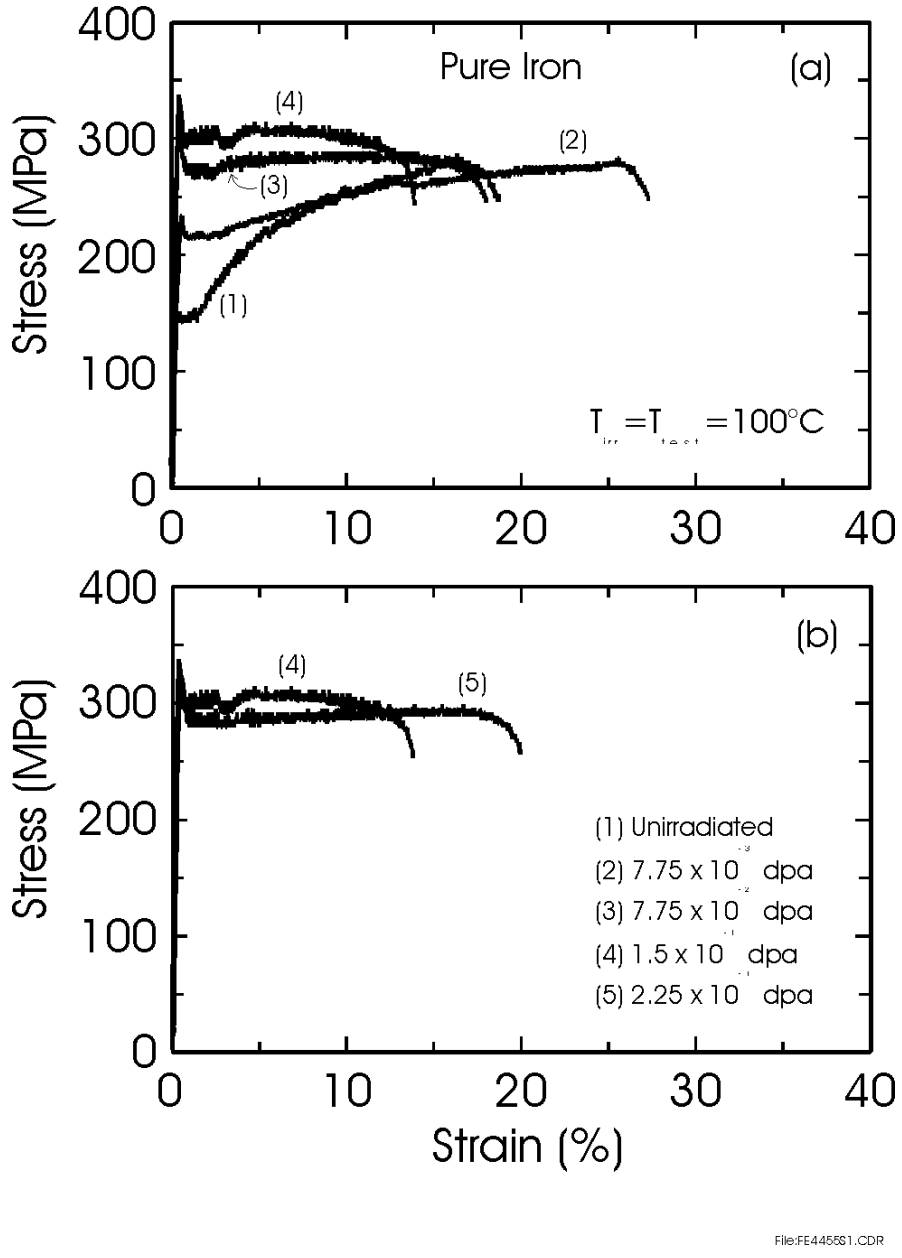


Figure 12. Stress-strain curves for pure iron irradiated at 100°C to different displacement dose levels and tested at 100°C in vacuum ($<10^{-5}$ torr). Note the irradiation-induced increase in the upper yield stress and yield drop and a decrease in the work hardening.

### 3.3.2 Dislocation Decoration and Cascade-Induced Source Hardening

*H. Trinkaus*, B.N. Singh and A.J.E. Foreman** (*Forschungszentrum Jülich, Germany, **AEA Technology, Harwell, England)*

Metals and alloys irradiated under cascade damage conditions at temperatures below the recovery stage V ($\sim$0.3 $T_m$) exhibit two important characteristics: (a) the grown-in dislocations get decorated by small interstitial loops formed during irradiations and (b) the irradiated materials deform in a localized fashion and suffer from plastic instability and loss of ductility. Recent analysis of these common observations demonstrated that the existing model known as dispersed barrier hardening model is not adequate to explain the experimental observations. Therefore, we have proposed a new model - cascade induced source hardening (CISH) model - which is based on the hypothesis that the small, glissile clusters of SIAs produced in the cascades are responsible for the formation of an "atmosphere" of SIA loops around the grown-in dislocations. Consequently, the grown-in dislocations are unable to act as dislocation sources. This leads to an increase in the level of applied stress necessary for the initiation of plastic flow (i.e. the upper yield stress).

In order to test the validity of the assumption of dislocation decoration, detailed calculations have been carried out to determine the mechanism of dislocation decoration by small loops. Calculations have shown that the phenomenon of dislocation decoration cannot be rationalized in terms of three-dimensionally diffusing single SIAs in the strain field of a grown-in dislocation. This interaction leads to a depletion (instead of an enhanced accumulation) not only in the compressive but also in the dilatational region of the dislocation. The analysis shows that the trapping and accumulation of SIAs near dislocations would require a restriction in the dimension of SIA migration which is most efficient in the case of a strictly one-dimensional motion. This requirement is easily fulfilled by the groups of coupled crowdions in the form of glissile perfect SIA loops produced in the cascades. The equipotential contour lines for the interaction between a perfect edge dislocation and perfect SIA loops and paths of glissile loops approaching the edge dislocation by glide and climb are shown in Figure 13.

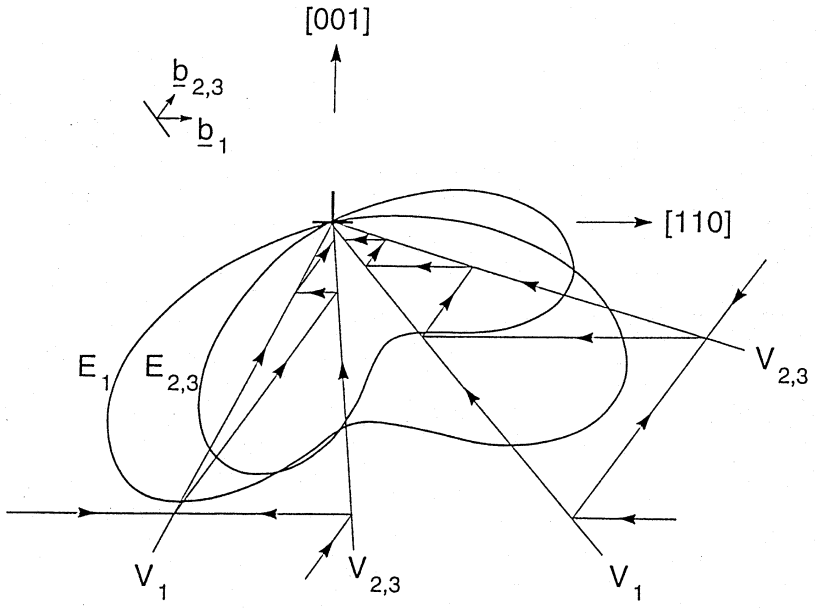


Figure 13. Equipotential lines for the interaction betwen a perfect edge dislocation and perfect SIA loops and paths for glissile loops for approaching the dislocation line by climb and glide.

It is further shown that the small loops trapped in the strain field of a dislocation may be detrapped by thermal activation. Before this occurs, the small loops may approach the dislocation by thermally activated changes in the Burgers vector and/or by conservative climb. Thus, the decoration of dislocations with loops requires that a single trapped loop is immobilized by other loops before it is detrapped from or absorbed by the edge dislocation. This requirement makes the dislocation decoration phenomenon dependent on the dislocation density, the loop production rate, the rate of Burgers vector change, the climb velocity and the irradiation temperature. A considerable amount of further work is needed to determine these dependencies quantitatively.

# 3.4 Underlying Technology

### 3.4.1 Post-irradiation Annealing and Defect Recovery

*M. Eldrup, B.N. Singh and P. Toft*

In an effort to further our understanding of the process involved in the defect recovery during post-irradiation annealing experiments, specimens of pure OFHC-copper and pure α-iron irradiated at 100 and 50°C, respectively, to different dose levels were investigated. Both copper and iron specimens were irradiated in annealed conditions. Specimens of both copper and α-iron were tensile tested in the as-irradiated condition as well as after post-irradiation annealing at 300°C for 50 h. Tensile tests were carried out at the irradiation temperature, whereas electrical

resistivity measurements were made at the ambient temperature (~23°C). Figure 14 illustrates the effect of the post-irradiation annealing treatment on the tensile deformation behaviour of copper specimens irradiated at 100°C to doses of 0.01, 0.1, 0.2 and 0.3 dpa. The results shown in Figure 14 illustrate the following three main effects of the post-irradiation annealing at 300°C for 50 h:

(i) the removal of the yield drop and plastic instability,

(ii) a significant reduction in the yield stress,

(iii) neither the yield stress nor the uniform elongation recover to the level observed in the unirradiated specimens.

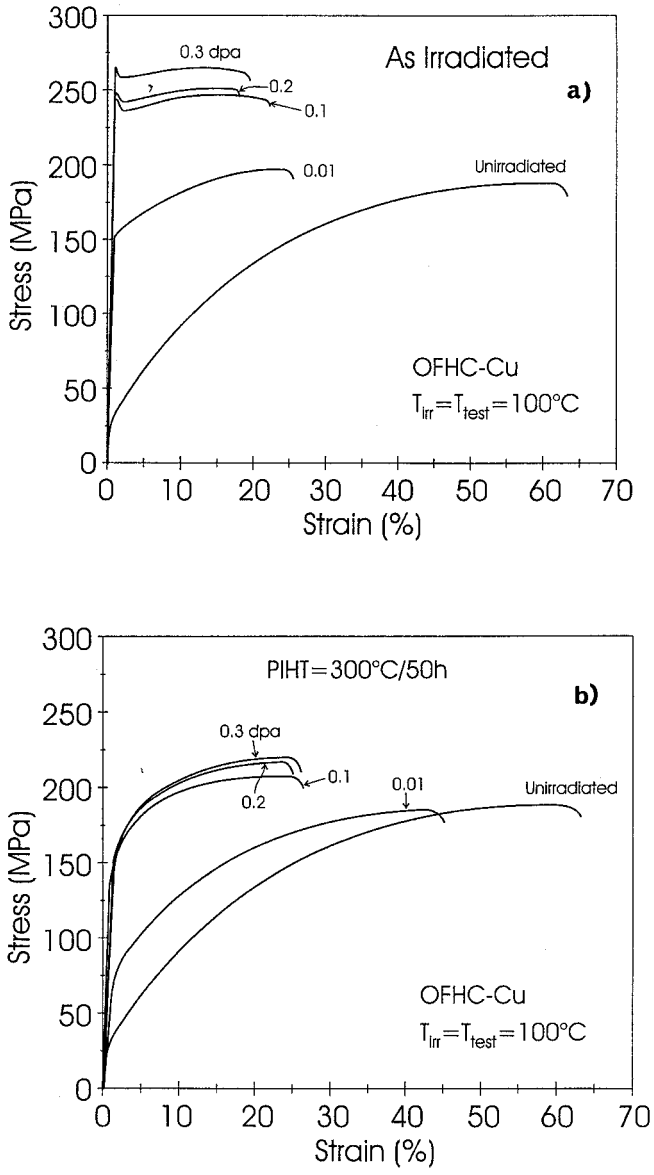


Figure 14. Stress-strain curves for OFHC-copper irradiated at 100°C to different doses and tested (a) in the as-irradiated condition and (b) after post-irradiation annealing at 300°C for 50 h. Note that the annealing eliminates the plastic instability but does not lead to a complete recovery of the ductility.

In parallel with tensile testing of neutron irradiated iron and copper, electrical conductivity measurements have been carried out on the tensile specimens. These were ~280 μm thick and ~3.0 mm wide along the gauge length which for the conductivity measurements was ~5 mm. The iron specimens were annealed at 650°C and copper at 550°C for 2 hours in a vacuum of $\sim 10^{-6}$ torr before reference measurements and neutron irradiation were carried out. The specimens were irradiated with fission neutrons in the DR-3 reactor at Risø at the temperatures 50°C (Fe) and 100°C (Fe and Cu) to dose levels up to 0.375 dpa (NRT). The damage rate was 4-5H$10^{-8}$ dpa/s. Some of the specimens were post-irradiation annealed at 300°C for 50 hours. Figure 15 a and b summarize the results of the conductivity measurements. All results are given as "Relative Conductivity", i.e. the measured conductivity, σ, divided by the conductivity of the metal in the as-heat treated condition, i.e. $\sigma_{Fe}$ (= 0.0986 $(\mu\Omega cm)^{-1}$, close to the nominal value of 0.103 $(\mu\Omega cm)^{-1}$) or $\sigma_{Cu}$ (= 0.592 $(\mu\Omega cm)^{-1}$, close to the nominal value of 0.589 $(\mu\Omega cm)^{-1}$).

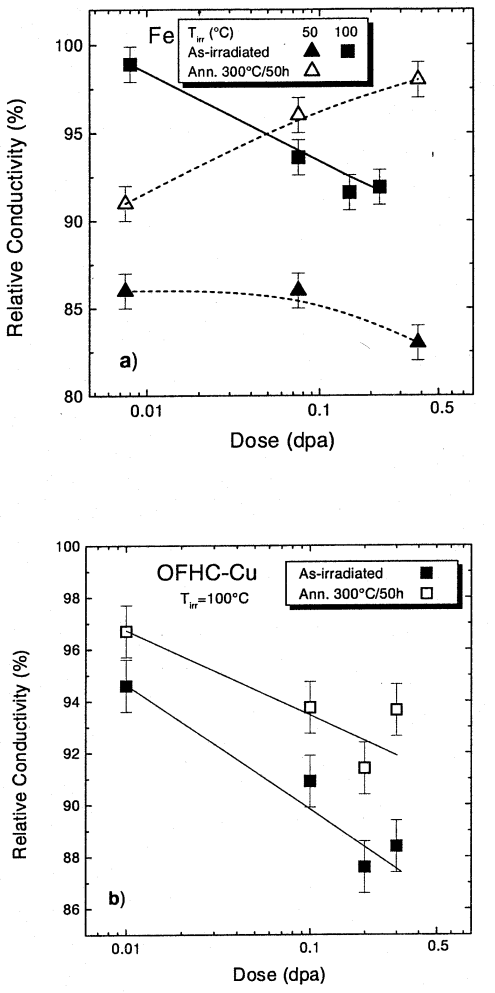


Figure 15. The electrical conductivity of neutron irradiated iron (a) and copper (b), relative to the conductivities for the un-irradiated materials, as functions of irradiation dose. Data are shown both for the as-irradiated state and after annealing at 300°C for 50 hours. The apparently different behaviour of the two materials is ascribed to differences in crystal structure and impurity content.

In iron, a clear difference is observed in the dose dependence of the conductivities for irradiations at 50°C and at 100°C (Figure 15a). Iron irradiated at 50°C shows a decrease in conductivity to 86% even at a low dose of 0.0075 dpa. Only a small decrease to 83% is observed up to 0.38 dpa. This behaviour is ascribed to the trapping of vacancies by impurity carbon atoms which are immobile at this temperature. For irradiation at 100°C, i.e. above the migration temperature for carbon (~70°C), the conductivity decreases only slightly to 99% at the lowest dose, but with increasing dose continues to decrease down to 92%, a dose dependence similar to the one observed for copper irradiated at 100°C (Figure 15b) and ascribed to the increasing density of radiation created defects and their clusters. The large difference in behaviour of iron irradiated at 50°C and 100°C illustrates the sensitivity of the electrical conductivity to impurities and the defect microstructure.

On annealing at 300°C of iron irradiated at 50°C, recovery of the defect structure takes place, resulting in an electrical conductivity that increases with dose (Figure 15a). Possibly this dose dependence must be associated with the influence of impurities other than carbon (e.g. nitrogen). In contrast to the iron, annealing of copper results in recovery of about one third of the conductivity loss at all doses. Thus, after annealing, the conductivity still decreases with dose (Figure 15b).

### 3.4.2 Effect of Recoil Energy on Defect Accumulation

*B.N. Singh, S.I. Golubov*) and H. Trinkaus**) (*)IPPE, Obninsk, Russia, **)Forschungszentrum Jülich, Germany)*

In the past, the effect of recoil energy on defect accumulation in the form, for example, of voids has not been treated explicitly. A close examination of the literature helps to identify two main reasons for this limitation. First, the vital information regarding the details (e.g. nature, efficiency and morphology) of defect production as a function of recoil energy did not become available until rather recently. The second reason is related to the fact that the earlier theories were based on homogeneous kinetics and mean field approach and were unable to treat the problem of defect accumulation under the condition when both glissile and sessile clusters of self-interstitial atoms (SIAs) are generated at higher recoil energies. Furthermore, up to a certain level of recoil energy, both the damage efficiency and the amount of SIA clusters produced during irradiation depends strongly on the damage energy.

The recently proposed Production Bias Model (PBM), on the other hand, is fully capable of treating the problem of intracascade clustering of SIAs and the glide of SIA clusters. In fact, one of the major predictions of the PBM is that the defect accumulation above the recovery stage V should be recoil energy dependent. In the present work, the effect of recoil energy on defect accumulation under 2.5 MeV electron, 3 MeV proton and fission neutron has been investigated. Calculations have been carried out in terms of PBM using one-dimensional glide of SIA clusters, sessile-glissile loop transformation and size distribution function. The calculated components of the irradiation-induced microstructure (i.e. size and density of SFT, SIA clusters and

voids) and their dose dependence for copper irradiated with 3 MeV protons and fission neutrons are found to be in very good agreement with the experimental results (e.g. see Figure 16). The void swelling behaviour observed under 2.5 MeV electron irradiation where defects are produced in the form of Frenkel pairs (i.e. no clusters of SIAs) can be clearly understood in terms of the standard rate theory and dislocation bias. The analysis of these results yields a dislocation bias of ~2%.

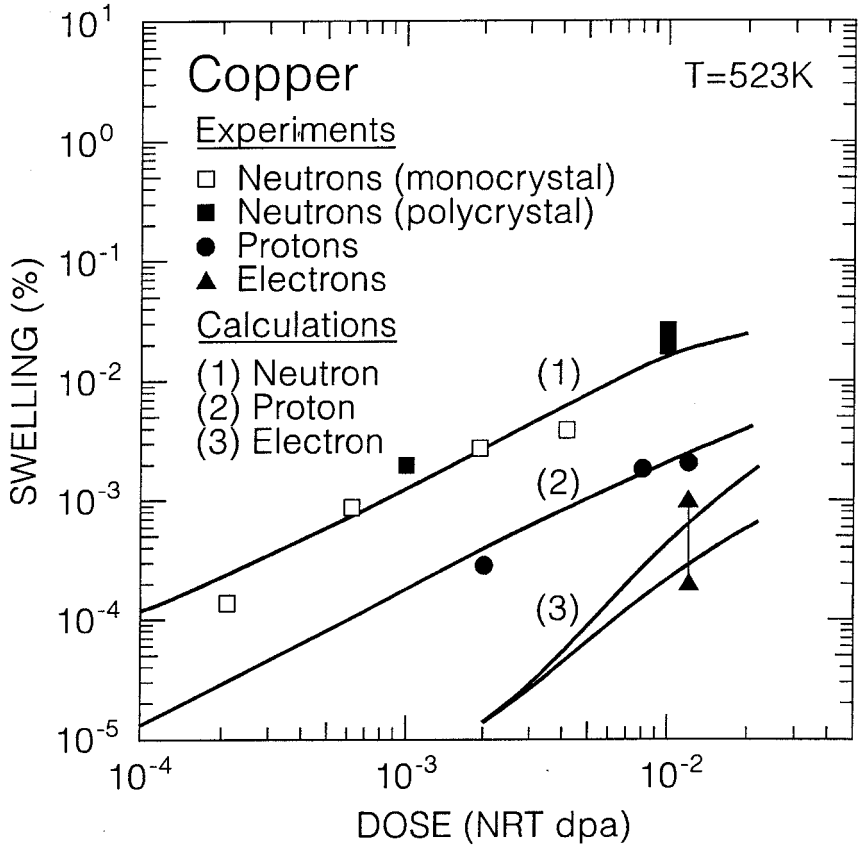


Figure 16. Effect of recoil energy on the dose dependence of void swelling in copper at 250°C calculated in terms of the Production Bias Model and comparison with experimental results.

### 3.4.3 Defect Accumulation and Radiation Hardening in Monocrystals of Mo and Mo-5% Re Alloy

*B.N. Singh, J.H.Evans*, A. Horsewell and P. Toft (* University of London, England)*

Tensile specimens and 3 mm diameter discs of monocrystals of pure molybdenum and Mo-5% Re alloy were irradiated in helium-filled capsules with fission neutrons in the DR-3 reactor at Risø. Irradiations were carried out at ~50$^{o}$C to displacement doses in the range of 5.4 x $10^{-4}$ to 1.6 x $10^{-1}$ dpa (displacement per atom). For comparison, polycrystalline specimens were also irradiated. Post-irradiation microstructures were quantitatively characterized using transmission electron microscopy (TEM). Both unirradiated and irradiated specimens were tensile tested at the ambient temperature. The microstructure of the irradiated and deformed specimens were also examined using TEM.

Monocrystals of both pure Mo and Mo-5% Re alloy suffer from plastic instability in the same way as do the polycrystals (see Figure 17). The occurrence of plastic instability suggests that up to a certain stress level dislocation sources remain locked. At the upper yield stress, a number of dislocation sources begin to operate and form “cleared” channels. In other words, the plastic deformation is localized and occurs only in these cleared channels. The analysis of the present results suggests that during irradiation under cascade damage conditions, gliding SIA clusters block the dislocation sources and thus prevents homogeneous plastic deformation. Consequently, the crack nucleation is no longer caused by plastic deformation. Instead, the crack must initiate at internal and/or external flows in the material. The interaction of these cleared channels with external surfaces or grain boundaries or intersections of these channels with each other may initiate cracks. Once initiated, the crack is likely to propagate rapidly through the material since the irradiated mateial is unable to deform plastically in homogeneous fashion. Consequently, the material fails in a brittle manner with intergranular clearage fracture (Figure 18).

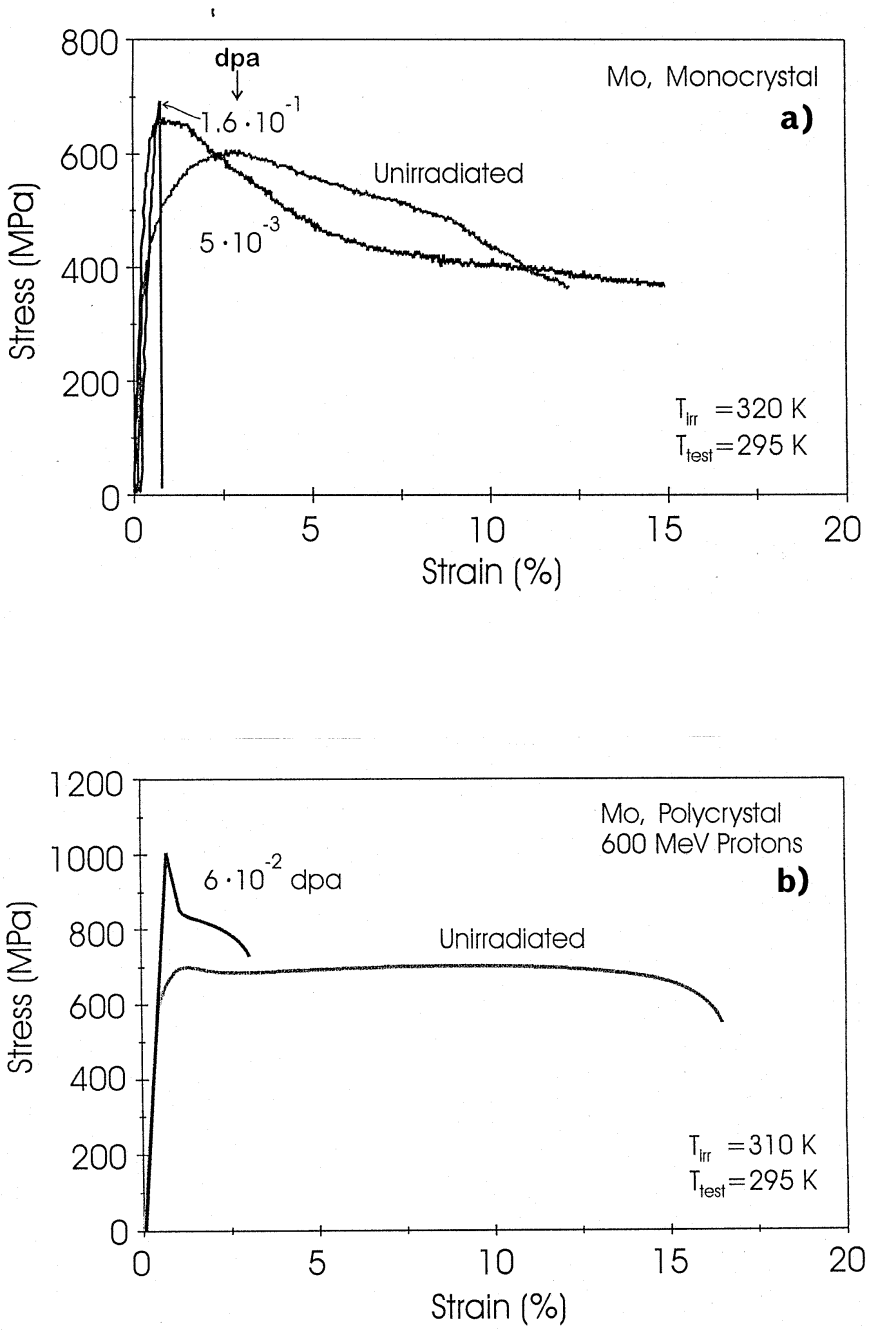


Figure 17. Stress-strain curves for the unirradiated and irradiated (a) monocrystals and (b) polycrystals of Mo irradiated at 50°C and tested at room temperature.

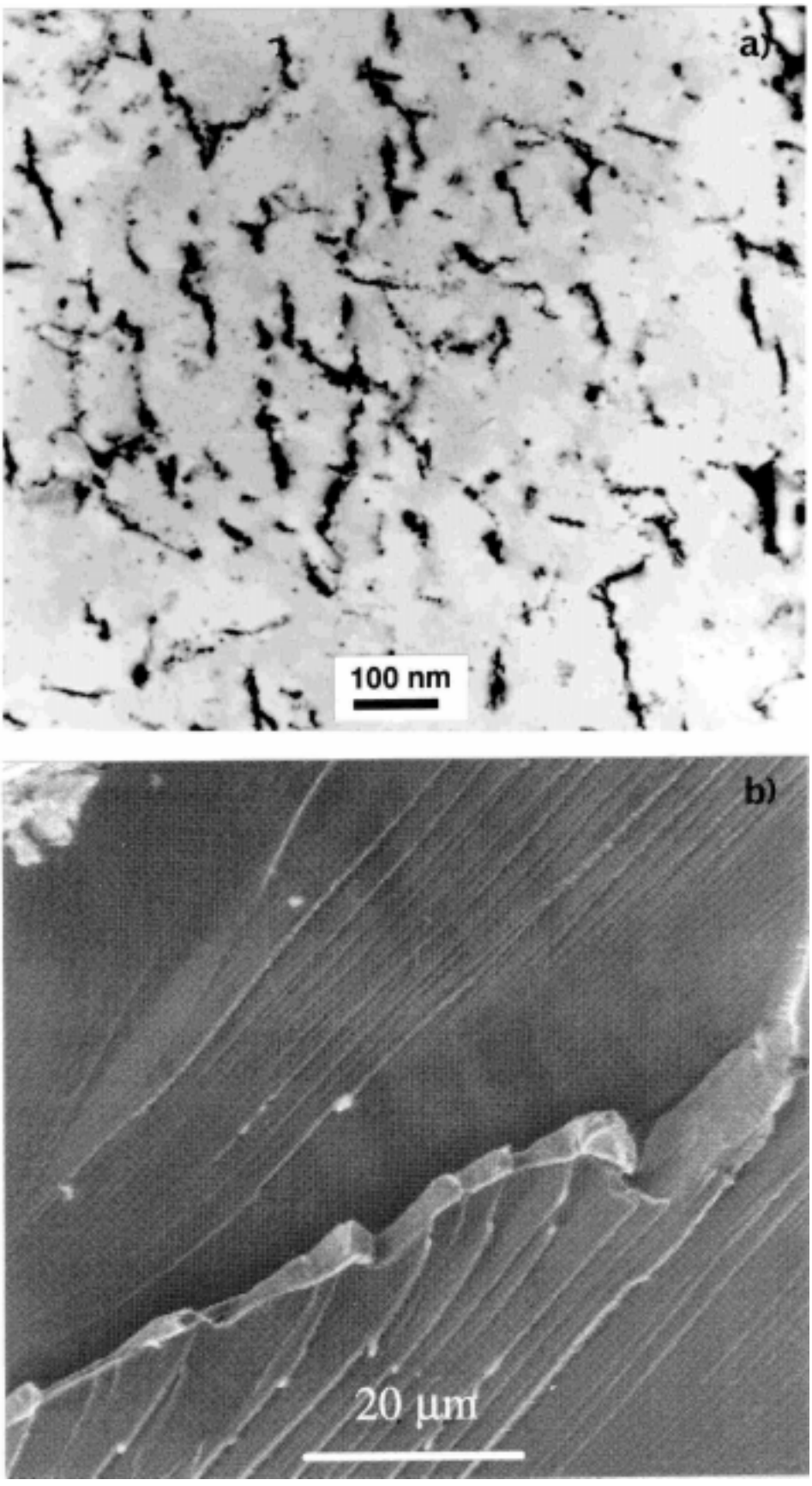


Figure 18. (a) Post deformation microstructure of Mo monocrystal irradiated at 50°C to a dose level of 0.16 dpa (NRT) showing lack of dislocation generation and (b) fractograph of the fracture surface of the same specimen showing cleavage fracture.

## 3.5 Participants in Fusion Technology

**Scientific Staff**
Eldrup, Morten (part time, ~ 70%)
Horsewell, Andy (part time, ~ 20%)
Singh, Bachu N
Toft, Palle (part time, ~ 60%)

**Technical Staff**
Lindbo, Jørgen (part-time, ~ 20%)
Nilsson, Helmer (part time, ~ 10%)
Olsen, Benny F
Pedersen, N.J. (part time, ~ 40%)

**Guest Scientists**
Edwards, D.J
Pacific Northwest National Laboratory, Richland, U.S.A

Golubov, S.I
Institute of Physics and Power Engineering, Obninsk, Russia

Heinisch, H.L
Pacific Northwest National Laboratory, Richland, U.S.A

## 3.6 Publications and Conference Contribution

### 3.6.1 International Publications

Almazouzi, A.; Diaz de la Rubia, T.; Ishino, S.; Lam, N.Q.; Singh, B.N.; Trinkaus, H.; Victoria, M.; Zinkle, S., Defect production, accumulation and materials performance in an irradiation environment. Summary. International workshop on defect production, accumulation and materials performance in an irradiation environment, Davos (CH), 2-8 Oct 1996. J. Nucl. Mater. (1997) v. 251 p. 291-294

Edwards, D.J.; Singh, B.N.; Toft, P.; Eldrup, M., Recent results on the neutron irradiation of ITER candidate copper alloys irradiated in DR-3 at 250(degrees)C to 0.3 dpa. In: Fusion materials semiannual progress report for the period ending December 31, 1996. (1997) p. 183-193

Eldrup, M.; Sanders, P.G.; Weertman, J.R., Positron annihilation study of the influence of grain size and purity on the annealing behaviour of nano-crystalline copper. 11. International conference on positron annihilation, Kansas City, MO (US), May 1997. Mater. Sci. Forum (1997) v. 255/257 p. 436-438

Eldrup, M.; Singh, B.N., Studies of defects and defect agglomerates by positron annihilation spectroscopy. J. Nucl. Mater. (1997) v. 251 p. 132-138

Heinisch, H.L.; Singh, B.N., Stochastic annealing simulation of intracascade defect interactions. International workshop on defect production, accumulation and materials performance in an irradiation environment, Davos (CH), 2-8 Oct 1996. J. Nucl. Mater. (1997) v. 251 p. 77-85

Singh, B.N.; Edwards, D.J.; Eldrup, M.; Toft, P., Effects of heat treatments and neutron irradiation on microstructures and physical and mechanical properties of copper alloys. J. Nucl. Mater. (1997) v. 249 p. 1-16

Singh, B.N.; Foreman, A.J.E.; Trinkaus, H., Radiation hardening revisited: Role of intracascade clustering. J. Nucl. Mater. (1997) v. 249 p. 103-115

Singh, B.N.; Golubov, S.I.; Trinkaus, H.; Serra, A.; Osetsky, Yu.N.; Barashev, A.V., Aspects of microstructure evolution under cascade damage conditions. International workshop on defect production, accumulation and materials performance in an irradiation environment, Davos (CH), 2-8 Oct 1996. J. Nucl. Mater. (1997) v. 251 p. 107-122

Trinkaus, H.; Singh, B.N.; Foreman, A.J.E., Mechanisms for decoration of dislocations by small dislocation loops under cascade damage conditions. J. Nucl. Mater. (1997) v. 249 p. 91-102

Trinkaus, H.; Singh, B.N.; Foreman, A.J.E., Segregation of cascade induced interstitial loops at dislocations: Possible effect on initiation of plastic deformation. International workshop on defect production, accumulation and materials performance in an irradiation environment, Davos (CH), 2-8 Oct 1996. J. Nucl. Mater. (1997) v. 251 p. 172-187

Wang, C.L.; Maurer, F.H.J.; Eldrup, M.; Pedersen, N.J., Free-volume properties and positronium formation in poly(vinyl acetate) and poly(methyl methacrylate). 11. International conference on positron annihilation, Kansas City, MO (US), May 1997. Mater. Sci. Forum (1997) v. 255/257 p. 387-389

### 3.6.2 Danish Reports

Singh, B.N.; Edwards, D.J.; Eldrup, M.; Toft, P., Effect of bonding and bakeout thermal cycles on the properties of copper alloys irradiated at 350 deg. C. Risø-R-971(EN) (1997) (ITER R&D Task No. T213) 44 p.

Singh, B.N.; Edwards, D.J.; Eldrup, M.; Toft, P., Pre- and post-irradiation properties of copper alloys at 250 deg. C following bonding and bakeout thermal cycles. Risø-R-937(EN) (1997) (ITER R&D Task No. T213) 55 p.

Singh, B.N.; Stubbins, J.F.; Toft, P., Fatigue performance of copper and copper alloys before and after irradiation with fission neutrons. Risø-R-991(EN) (1997) (ITER R&D Task No. T213) 42 p.

### 3.6.3 Foreign Books and Reports

Almazouzi, A.; Victoria, M.; Singh, B.N.; Diaz de la Rubia, T. (eds.), Defect production, accumulation and materials performance in an

irradiation environment. Proceedings. International workshop on defect production, accumulation and materials performance in an irradiation environment, Davos (CH), 2-8 Oct 1996. (Elsevier, Amsterdam, 1997) (J. Nucl. Mater., vol. 251) 300 p.

Jean, Y.C.; Eldrup, M.; Schrader, D.M.; West, R.N. (eds.), Positron annihilation. IPCA-11. 11. international conference on positron annihilation, Kansas City, MO (US), May 1997. (Trans Tech Publications, Zürich, 1997) (Mater. Sci. Forum, 255/257) 852 p.

### 3.6.4 Conference Lectures

Kirkegaard, P.; Eldrup, M., Regularization and simulation techniques for reconstructing particle and cavity distributions in TEM. In: World congress on scientific computation, modelling and applied mathematics. Vol. 5: Systems engineering. 15. IMACS world congress, Berlin (DE), 24-29 Aug 1997. Sydow, A.; Schäfer, R.-P.; Rufeger, W.; Lehmann, H. (eds.), (Wissenschaft und Technik Verlag, Berlin, 1997) p. 501-506

Singh, B.N.; Toft, P., Pre- and post-irradiation properties of pure iron and low activation steels. In: Proceedings of the second Milestone meeting of European laboratories on the development of ferritic/martensitic steels for fusion technology. 2. Milestone meeting of European laboratories on the development of ferritic/martensitic steels for fusion technology, Karlsruhe (DE), 9-10 Sep 1996. Daum, E.; Ehrlich, K.; Schirra, M. (eds.), (1997) p. 47-51

### 3.6.5 Unpublished Lectures

Edwards, D.J.; Singh, B.N.; Toft, P.; Eldrup, M., Effect of bonding and bakeout thermal cycles on the properties of copper alloys irradiated at 100 degr.C. Poster presentation at the ICFRM-8, Sendai (JP), 26-31 Oct 1997. Unpublished.

Eldrup, M., Positronium localization of non-thermalization in molecular crystals. Foredrag ved Department of Basic Sciences, University of Tokyo, Tokyo (JP), 4 Nov 1997. Unpublished.

Eldrup, M.; Singh, B.N., Influence of composition, heat treatment and neutron irradiation on the electrical conductivity of copper alloys. Poster presentation at the ICFRM-8, Sendai (JP), 26-31 Oct 1997. Unpublished.

Golubov, S.I.; Singh, B.N.; Trinkaus, H., Calculations of recoil energy effects on defect accumulation in terms of production bias and loop glide. Poster presentation at the ICFRM-8, Sendai (JP), 26-31 Oct 1997. Unpublished.

Heinisch, H.; Singh, B.N., Stochastic annealing simulation of copper under continuous neutron irradiation. Poster presentation at the ICFRM-8, Sendai (JP), 26-31 Oct 1997. Unpublished.

Karjalainen-Roikonen, P.; Pyykkönen, M.; Tähtinen, S.; Singh, B.N.; Toft, P., Effects of neutron irradiation on fracture toughness and tensile behaviour of copper alloys and their joints with stainless steel. Poster presentation at the ICFRM-8, Sendai (JP), 26-31 Oct 1997. Unpublished.

Singh, B.N., Results and analysis of screening and post-irradiation annealing experiments on copper alloys. ITER working meeting on development and irradiation tests of Cu/SS and Be/Cu/SS joints (tasks T212 and T213), Garching (DE), 24-26 Mar 1997. Unpublished.

Singh, B.N., Status and current conclusions of ongoing ITER task T-213 on copper and copper alloys. EUHT/JCT review meeting on materials and joining technology tasks, Risø (DK), 19-20 Nov 1997. Unpublished.

Singh, B.N., Recent results on effects of irradiation on physical and mechanical properties of copper alloys. Workshop on materials and joints for in-vessel components, Garching (DE), 1-5 Dec 1997. Unpublished.

Singh, B.N., Evidence of spectral and rate effects on damage accumulation in metals and alloys. IFMIF-users group meeting, IMR, Tohoku University, Sendai (JP), 1 Nov 1997. Unpublished.

Singh, B.N., Radiation hardening and plastic instability in neutron irradiated Mo and Mo-alloys. IEA international workshop on refractory metals and alloys for fusion applications, Sendai (JP), 24-25 Oct 1997. Unpublished.

Singh, B.N., Damage production, accumulation and consequences: A review. International workshop on radiation damage in metals, Liverpool (GB), 17-18 Apr 1997. Unpublished.

Singh, B.N., Consequences of atomic displacements in crystalline solids. Seminar given at the Hong Kong Polytechnic University, Hong Kong (CN), 6 Nov 1997. Unpublished.

Singh, B.N., Impacts of damage production and accumulation on materials performance in irradiation environment. Invited talk at 8. International conference on fusion reactor materials (ICFRM-8), Sendai (JP), 26-31 Oct 1997. Unpublished.

Singh, B.N.; Evans, J.H.; Horsewell, A.; Toft, P., Effects of neutron irradiation on microstructure and deformation behaviour of mono- and polycrystalline molybdenum and its alloys. Poster presentation at the ICFRM-8, Sendai (JP), 26-31 Oct 1997. Unpublished.

Singh, B.N.; Horsewell, A.; Toft, P., Microstructure and deformation behaviour of neutron irradiated iron and low activation ferritic/martensitic steels. IEA workshop on reduced activation ferritic/martensitic steels, Tokyo (JP), 3-4 Nov 1997. Unpublished.

Singh, B.N.; Horsewell, A.; Toft, P., Effects of neutron irradiation on microstructure and mechanical properties of pure iron and low activation steels. Poster presentation at the ICFRM-8, Sendai (JP), 26-31 Oct 1997. Unpublished.

Stubbins, J.F.; Singh, B.N.; Toft, P., Fatigue performance of copper and copper alloys before and after irradiation to 0.3 dpa at 50 and 100 degr.C. Poster presentation at the ICFRM-8, Sendai (JP), 26-31 Oct 1997. Unpublished.

# 4. Socio-Economic Research on Fusion (SERF)

## 4.1 Macrotasks

The Systems Analysis Department at Risø National Laboratory is contributing in three macro-tasks in the programme for Socio-Economic Research on Fusion (SERF):

- Macro task SE0: Development of long term scenarios.
- Macro task E1: Production costs of energy technologies
- Macro task E2: External costs and benefits of energy technologies

Concerning macro task SE0, Risø National Laboratory is mainly contributing with analysis of existing long-term studies. With starting point in the WEC study, identification of a number of key parameters has been initiated. Special emphasis is put on the development of energy demand, especially demand for electricity and heat. Finally, the long-term use of renewable energy technologies are addressed, especially the use of wind energy.

The Risø contribution in macro task E1 is mainly related to the long-term cost assessment of renewables, especially wind energy and photovoltaics. A cost analysis for wind energy has been carried out in considerable details. The analysis has included land sited turbines as well as off shore turbines, which might be expected to play a significant role in the energy systems in the long term. In the next phase of the study the very long-term development of wind power (year 2030-75) will be adressed. What concerns photovoltaics the analysis is expected to start in late March or beginning of April 1998.

Concerning macro task E2, Risø is responsible for the evaluation of external costs for wind energy and photovoltaics using the ExternE methodology and the comparison calculated for these renewable energy sources with those from fusion. The work until now has been concentrated on the externalities for wind energy. Externalities have been monetised for an offshore wind farm as well as for a wind farm on land. The work will continue in this field regarding photovoltaics.

## 4.2 Scientific staff

Poul Erik Morthorst
Lotte Schleisner

**Bibliographic Data Sheet** **Risø-R-1070(EN)**

Title and author(s)

Association Euratom – Risø National Laboratory
Annual Progress Report for 1997
Edited by J. P. Lynov and B. N. Singh


| ISBN | ISSN |
|---|---|
| 87-550-2438-6 | 0106-2840 |
| 87-550-2439-4 (Internet) | 1396-3449 |

| Dept. or group | Date |
|---|---|
| Optics and Fluid Dynamics Department | November 1998 |

| Pages | Tables | Illustrations | References |
|---|---|---|---|
| 60 | 5 | 30 | 12 |



Abstract (max. 2000 char.)

The programme of the Research Unit of the Fusion Association Euratom - Risø National Laboratory covers work in fusion plasma physics and in fusion technology. The fusion plasma physics group has activities within development of laser diagnostics for fusion plasmas and studies of nonlinear dynamical processes related to electrostatic turbulence and turbulent transport in magnetised plasmas. The activities in technology cover investigations of radiation damage of fusion reactor materials. These activities contribute to the Next Step, the Long-term and the Underlying Fusion Technology programme. The technology activities also include contibutions to macrotasks carried out under the programme for Socio-Economic Research on Fusion (SERF). A summary is presented of the results obtained in the Research Unit during 1997.



Descriptors INIS/EDB

LASER DOPPLER ANEMOMETERS; MAGNETIC CONFINEMENT; NON-LINEAR PROBLEMS; NUMERICAL SOLUTION; PELLET INJECTION; PHYSICAL RADIATION EFFECTS; PLASMA DIAGNOSTICS; PLASMA SCAPE-OFF LAYER; PLASMA SIMULATION; PROGRESS REPORT; RISOE NATIONAL LABORATORY; THERMONUCLEAR REACTOR MATERIALS; TOKAMAK DEVICES; TURBULENCE; VORTICES

Available on request from:
Information Service Department, Risø National Laboratory (Afdelingen for Informationsservice, Forskningscenter Risø)
P.O. Box 49, DK-4000 Roskilde, Denmark
Phone (+45) 4677 4677, ext. 4004/4005; fax (+45) 4677 4013